



Published in final edited form as:

Nat Neurosci. 2023 August ; 26(8): 1328–1338. doi:10.1038/s41593-023-01374-9.

Globally reduced *N*⁶-methyladenosine (m⁶A) in C9ORF72-ALS/FTD dysregulates RNA metabolism and contributes to neurodegeneration

Yini Li^{1,2,†}, Xiaoyang Dou^{3,4,†}, Jun Liu^{3,4,5,†}, Yu Xiao^{3,4,†}, Zhe Zhang^{1,2}, Lindsey Hayes^{2,6}, Rong Wu^{1,2}, Xiujuan Fu^{1,2}, Yingzhi Ye^{1,2,7}, Bing Yang⁸, Lyle W. Ostrow⁹, Chuan He^{3,4,10,*}, Shuying Sun^{1,2,11,12,*}

¹Department of Physiology, Johns Hopkins University School of Medicine, Baltimore, MD 21205, USA.

²Brain Science Institute, Johns Hopkins University School of Medicine, Baltimore, MD 21205, USA.

³Department of Chemistry and Institute for Biophysical Dynamics, The University of Chicago, Chicago, IL 60637, USA.

⁴Howard Hughes Medical Institute, Chicago, IL 60637, USA.

⁵Present: State Key Laboratory of Protein and Plant Gene Research, School of Life Sciences, Peking-Tsinghua Center for Life Sciences, Peking University, Beijing 100871, China.

⁶Department of Neurology, Johns Hopkins University School of Medicine, Baltimore, MD 21205, USA.

⁷Cellular and Molecular Physiology Graduate Program, Johns Hopkins University School of Medicine, Baltimore, MD 21205, USA.

⁸Laboratory of Cellular and Developmental Biology, NIDDK Intramural Research Program, Bethesda, MD 20892, USA.

⁹Department of Neurology, Lewis Katz School of Medicine at Temple University, Philadelphia, PA 19122, USA

¹⁰Department of Biochemistry and Molecular Biology, The University of Chicago, Chicago, IL 60637, USA.

This work is licensed under a Creative Commons Attribution 4.0 International License, which allows reusers to distribute, remix, adapt, and build upon the material in any medium or format, so long as attribution is given to the creator. The license allows for commercial use.

*Corresponding author. shuying.sun@jhmi.edu (S.S.); chuanhe@uchicago.edu (C.H.).

†These authors contributed equally to this work.

Author contributions

Y.L., X.D., C.H. and S.S. contributed to the overall design of the study and wrote the manuscript. Y.L. performed most molecular and cellular biology experiments with help from Y.X., J.L., Z.Z., R.W., X.F., and Y.Y., under the mentorship of S.S. and C.H. X.D. and Y.L. performed bioinformatic analysis of the high-throughput sequencing data. B.Y. performed blinded analysis of glutamate excitotoxicity. L.H. performed GP ELISA assay and analysis. L.W.O. advised on patient samples and provided key reagents.

Ethics Declarations

C.H. is a scientific founder, a member of the scientific advisory board and equity holder of Afema Bio, Inc. and AccuaDX Inc., a scientific cofounder and equity holder of Accent Therapeutics, Inc., and a member of the scientific advisory board of Rona Therapeutics.

¹¹The Solomon H. Snyder Department of Neuroscience, Johns Hopkins University School of Medicine, Baltimore, MD 21205, USA.

¹²Department of Pathology, Johns Hopkins University School of Medicine, Baltimore, MD 21205, USA.

Abstract

Repeat expansion in *C9ORF72* is the most common genetic cause of amyotrophic lateral sclerosis (ALS) and frontotemporal degeneration (FTD). Here, we show that *N*⁶-methyladenosine (m⁶A), the most prevalent internal mRNA modification, is downregulated in *C9ORF72*-ALS/FTD patient-derived iPSC-differentiated neurons and postmortem brain tissues. The global m⁶A hypomethylation leads to transcriptome-wide mRNA stabilization and upregulated gene expression, particularly for genes involved in synaptic activity and neuronal function. Moreover, the m⁶A modification in the *C9ORF72* intron sequence upstream of the expanded repeats enhances RNA decay via the nuclear reader YTHDC1, and the antisense RNA repeats can also be regulated through m⁶A modification. The m⁶A reduction increases the accumulation of repeat RNAs and the encoded poly-dipeptides, contributing to disease pathogenesis. We further demonstrated that by elevating m⁶A methylation we could significantly reduce repeat RNA levels from both strands and the derived poly-dipeptides, rescue global mRNA homeostasis, and improve survival of *C9ORF72*-ALS/FTD patient iPSC-derived neurons.

Introduction

Dysfunction of RNA metabolism has emerged as key player in multiple neurological disorders¹. Amyotrophic lateral sclerosis (ALS), a disease of motor neuron degeneration and motor symptoms, is increasingly recognized to have clinical, pathological and genetic overlaps with frontotemporal dementia (FTD), a neurodegenerative disease characterized by behavioral and language dysfunction². Pathological inclusions and/or causative genetic mutations in several RNA-binding proteins (RBP) are widely found in the two diseases, such as TDP-43, FUS/TLS, ATXN2, MATR3 and hnRNP family proteins³. Alternatively, the RNA-mediated toxicity could also arise from microsatellite repeat expansions². The most common genetic cause of both ALS and FTD is the hexanucleotide GGGGCC repeat expansion in the first intron of the *C9ORF72* gene². The repeat-containing RNAs form nuclear granules that could disturb RBP functions, and encode multiple dipeptide repeat (DPR) proteins with various toxicities⁴. Therefore, it is important to understand how the dysregulation of RNA metabolisms contributes to disease mechanisms.

In previous efforts to identify genetic modifiers of DPR production via a genome-wide CRISPR-Cas9 knockout screen, we found core components of the m⁶A writer complex, METTL3, and METTL14, as suppressors of DPR production⁵. *N*⁶-methyladenosine (m⁶A) is the most prevalent internal modification in eukaryotic mRNA^{6,7}. It is one of the few reversible RNA modifications that regulates RNA metabolism. m⁶A is installed by the “writer” methyltransferase complex composed of core subunits METTL3 and METTL14⁸, and can be removed by the “eraser” protein, FTO or ALKBH5 demethylase⁹⁻¹¹. Proteins that selectively recognize m⁶A-marked RNA, namely “readers”, showed distinct and

overlapping functions in modulating multiple steps of RNA processing, including splicing, degradation and translation, which is recognized as epitranscriptomic regulation^{9,12-15}. It is noted that m⁶A in the nervous system showed the highest abundance⁷ and strongest specificity¹⁶ compared to other tissues. Disruption of the components of m⁶A pathway impaired the development and function of the nervous system¹⁷. These indicate the importance of the m⁶A-mediated epitranscriptome in preserving neuronal integrity.

Here, we discovered that m⁶A RNA modification is abnormally reduced in C9ORF72-ALS/FTD. This m⁶A hypomethylation leads to transcriptome-wide gene expression dysregulation and increases the accumulation of both sense and antisense repeat RNAs and DPRs. Restoration of the m⁶A level by modulating either methyltransferase or demethylase can rescue the disease-related phenotypes. Our findings reveal a novel layer of RNA regulation that plays a critical role in the pathogenic mechanism of neurodegeneration.

Results

The m⁶A RNA modification is downregulated in C9ORF72-ALS/FTD

We analyzed the public proteomic data from Answer ALS and NeuroLINC, and found that the expression levels of m⁶A pathway components, especially the methyltransferases METTL3 and METTL14 in the “writer” complex, were markedly downregulated in C9ORF72-ALS/FTD patient-derived induced pluripotent stem cell (iPSC)-differentiated spinal neurons (iPSNs) (Fig. 1a and Extended Data Fig. 1a,b). Consistently, we also observed reduction of METTL3 and METTL14 in multiple additional patient iPSN lines in our lab (Fig. 1b,c and Extended Data Fig. 1c). We confirmed the difference was not due to the variation of neuron maturation or purity between control and patient lines (Extended Data Fig. 1d). Interestingly, no expression changes of *METTL3/14* were observed in patient iPSCs and lymphoblast cells (Fig. 1b,c), suggesting probable neuron-specific downregulation of the m⁶A methyltransferase components. Furthermore, the METTL3 and METTL14 levels also decreased in C9ORF72-ALS/FTD patient postmortem brain tissues (Extended Data Fig. 2a-c). We further quantified the m⁶A/A ratio in purified mRNAs using the ultra-high-performance liquid chromatography-tandem mass spectrometry (UHPLC-QQQ-MS/MS) method¹⁸. The m⁶A level was dramatically downregulated in both C9ORF72-ALS/FTD iPSNs and multiple regions of patient postmortem brain (Fig. 1d,e). Altogether, this indicates the profound dysregulation of m⁶A pathway in C9ORF72-ALS/FTD patients, which could likely perturb mRNA metabolism globally. Interestingly, the proteomic data suggested iPSNs of sporadic ALS also have reduced expression of the m⁶A writer components in comparison to the controls (Extended Data Fig. 3a,b), and the m⁶A abundance was found to be reduced in sporadic ALS patient postmortem tissues (Extended Data Fig. 3c). We focused on the C9ORF72-ALS/FTD in this work, which could shed light on future studies of sporadic diseases.

The repeat RNA downregulates METTL3 and METTL14 expression

We examined whether the C9ORF72 repeat expansion can affect the METTL3 and METTL14 expression level via gain of toxicity. As the m⁶A reduction was only observed in differentiated iPSNs, we performed the experiments in the human i³Neuron system, in which

the engineered human iPSC line contains doxycycline-inducible neurogenin-2 (NGN2) and can be differentiated into cortical neurons with high efficiency and homogeneity¹⁹. We expressed the 160× GGGGCC repeats or 50× GA or GR poly-dipeptides encoded by randomized codons in the differentiated i³Neurons via lentiviral transduction, and examined the endogenous *METTL3* and *METTL14* levels (Extended Data Fig. 4a). We found that the expression of GGGGCC repeats was sufficient to induce the reduction of the two methyltransferases (Extended Data Fig. 4b). The expression of DPRs from randomized codons did not have significant effect (Extended Data Fig. 4b), even though they were abundantly expressed in the neurons, confirmed by both bioluminescent assay of the N-terminal HiBiT tag and immunofluorescence of the C-terminal FLAG tag of GFP and DPRs (Extended Data Fig. 4c,d). It is noted that poly-GR had lower expression level than poly-GA in the i³Neurons (Extended Data Fig. 4c), which is in agreement with the observation in patients^{20,21}. Overall, this result indicates that the repeat RNA triggers the m⁶A dysregulation in C9ORF72 patient neurons.

Transcriptome-wide m⁶A hypomethylation in C9ORF72-ALS/FTD

Given the prevalence of m⁶A modification in mRNAs, we examined whether the m⁶A reduction leads to global mRNA metabolism changes, which could contribute to neurodegeneration in C9ORF72-ALS/FTD. We performed m⁶A RNA immunoprecipitation (MeRIP) coupled with high-throughput sequencing to map the transcriptome-wide m⁶A sites and compared the differences between control and patients using both iPSNs and postmortem motor cortex (MCTX) samples. About 30,000 m⁶A peaks were identified per group (Extended Data Fig. 5a), with enrichment of the GGACU consensus motif (Extended Data Fig. 5b). As expected, the peaks are abundant in coding sequences (CDS) and 3' untranslated regions (3' UTRs), especially enriched near the stop codons (Extended Data Fig. 5c). The C9ORF72-ALS/FTD neurons presented different m⁶A profiles from controls (Extended Data Fig. 5d), and there were significantly more hypomethylated peaks in C9 patient iPSNs and motor cortex tissues (Fig. 2a,b). The hypomethylated genes identified in iPSNs and postmortem motor cortex shared considerable overlaps (Fig. 2c), which were highly enriched in synaptic and neuronal functions (Fig. 2d and Extended Data Fig. 5e). Together, the MeRIP-seq confirmed the global m⁶A reduction and revealed the transcriptome-wide hypomethylation in C9ORF72-ALS/FTD patient iPSNs and postmortem tissues.

Global m⁶A hypomethylation dysregulates gene expression

We next assessed the potential impact of m⁶A hypomethylation on mRNA expression in C9ORF72-ALS/FTD by RNA-seq analysis (Extended Data Fig. 6a,b). Based on the m⁶A changes in C9 patients (Fig. 2a,b), we categorized transcripts into hypomethylated (hypo-m⁶A) and non-hypomethylated (non-hypo-m⁶A) groups. We found that the transcripts with hypomethylation exhibited significantly upregulated expression levels in C9ORF72-ALS/FTD patient iPSNs and motor cortices, while the non-hypomethylated transcripts tend to show no significant differences between patient and control (Fig. 2e,f). We validated several candidate genes. Indeed, the reduced m⁶A mark on the transcripts correlated with increased gene expression in patients iPSNs and motor cortices (Fig. 2g-i). To examine whether the m⁶A hypomethylation leads to prolonged mRNA half-life that contributes to

the gene upregulation, we measured the RNA decay rate in control and patient iPSNs. The neurons were treated with actinomycin D to halt de novo transcription, and RNAs were collected 0, 3, and 6 hours after treatment for RNA-seq to quantify the transcriptome-wide mRNA half-life. We identified that the hypomethylated transcripts in C9ORF72-ALS iPSNs exhibited significantly increased half-life compared to control iPSNs (Fig. 3a,b).

YTHDF2 is an m⁶A “reader” known to facilitate degradation of m⁶A-marked mRNAs in the cytoplasm^{13,15}. We performed YTHDF2 RNA immunoprecipitation (RIP) sequencing to identify its binding targets in iPSNs (Fig. 3c,d and Extended Data Fig. 6c). We identified that a significant proportion of the hypomethylated transcripts were bound by YTHDF2 (Fig. 3e), and the half-life of YTHDF2 mRNA targets were significantly increased in the C9ORF72-ALS/FTD iPSNs compared to the control (Extended Data Fig. 6d). Many hypomethylated YTHDF2 target gene transcripts with increased half-life were linked to synapse and neuronal functions (Extended Data Fig. 6e). Altogether, these results reveal that the m⁶A hypomethylation in mRNAs hinders the proper decay of transcripts majorly important for synaptic functions in C9ORF72-ALS/FTD, potentially contributing to neuronal dysfunction and degeneration.

m⁶A in the repeat-containing intron modulates DPR production

Besides global mRNAs, we also specifically examined the effect of m⁶A reduction on C9ORF72 repeat RNA metabolism. We previously found that the spliced intron containing the expanded (GGGGCC)_n repeats is exported to cytoplasm and subjected to the repeat-associated non-AUG (RAN) translation in all the three reading frames (poly-GA, poly-GP, poly-GR)^{22,23}. We identified m⁶A methyltransferase components as suppressors of DPR production by an unbiased CRISPR screen⁵. We first validated the effect using the established HeLa Flp-In dual luciferase reporter systems, in which the NanoLuc luciferase is generated through RAN translation of C9ORF72 GGGGCC repeats (C9R-NLuc)^{5,22}. In both the splicing reporter, in which the C9R-NLuc is located in the *C9ORF72* intron (Fig. 4a), and the monocistronic mRNA reporter (Fig. 4b), knockdown of METTL14 significantly increased the DPR proteins from all the reading frames (Fig. 4c-e). This suggests the m⁶A modification can modulate DPR production, and this effect is independent of splicing.

The intronic sequence upstream of the repeat expansion contains several m⁶A consensus motifs. Indeed, the MeRIP-seq revealed m⁶A peaks in the *C9ORF72* intron regions surrounding the repeats (Extended Data Fig. 7a). MeRIP coupled with RT-qPCR showed enrichment of the *C9R-NLuc* RNA but not the negative control (Fig. 4f). Furthermore, deletion of the intronic sequence (intron) upstream of the repeats eliminated the DPR upregulation induced by METTL14 reduction (Fig. 4b,d). Altogether, this reveals that the m⁶A modification in the C9 intron can regulate the DPR production from the repeat-containing RNA.

We further validated the results in human i³Neurons. We expressed the luciferase reporters and shRNA targeting METTL14 in differentiated i³Neurons via lentiviral transduction (Fig. 4g). Similar to the observation in HeLa cells, reduction of METTL14 increased the levels of all the three DPR proteins, and this effect was diminished in the intron mutants (Fig.

4h, Extended Data Fig. 7b). This demonstrates that the m⁶A modification-mediated DPR regulation mechanism is conserved in neurons.

YTHDC1-NEXT regulates the stability of *C9ORF72* repeat RNA

To decipher the molecular mechanism of the DPR regulation by m⁶A modification, we examined the repeat-containing RNA level. There was increased *C9R-NLuc* RNA in the intron reporter cells compared to the wild type control (Extended Data Fig. 7c), suggesting the m⁶A modification in the intron modulates the repeat RNA accumulation. Indeed, the *C9R-NLuc* RNA was upregulated upon METTL14 knockdown in both HeLa and i³Neuron reporter systems (Fig. 5a and Extended Data Fig. 7d), consistent with the DPR changes (Fig. 4d,h). As the steady-state RNA level can be influenced by the RNA turnover rate, we examined two m⁶A “readers” with well-documented RNA decay function: YTHDC1, primarily responsible for the degradation of non-coding RNAs in the nucleus²⁴; and YTHDF2, predominantly in the cytoplasm for mRNA decay^{13,15}. We found that knockdown of YTHDF2 did not induce any changes (Extended Data Fig. 8a-c), but knockdown of YTHDC1 significantly increased the RNA and DPR levels of *C9R-NLuc* in both HeLa cells and i³Neurons (Fig. 5b-d and Extended Data Fig. 8d-f), consistent with the effect by METTL14 reduction (Fig. 4d,h,5a and Extended Data Fig. 7d). The elevation of DPRs by YTHDC1 knockdown was abolished in the intron-deletion mutant reporter (Extended Data Fig. 8f). In addition, the upregulated RNA level was in line with the increased half-life (Fig. 5e). Co-immunoprecipitation showed that YTHDC1 interacts with ZCCHC8, the core component of the Nuclear Exosome Targeting (NEXT) complex²⁵ in iPSNs (Fig. 5f). Knockdown of ZCCHC8 significantly increased DPR production, and the effect was dependent on the intronic sequence preceding the repeats (Fig. 5g,h and Extended Data Fig. 8g,h). Altogether, the results from both HeLa cells and i³Neurons support that YTHDC1 mediates the decay of the m⁶A-marked *C9* intron RNA by targeting to the NEXT complex. In *C9ORF72*-ALS/FTD, the hypomethylation of the repeat-containing intronic RNA (Extended Data Fig. 7a,9a) and the reduction of YTHDC1 protein (Extended Data Fig. 9b,c) could synergistically decelerate the RNA degradation, contributing to the increased accumulation of repeat RNA and DPRs with various toxicity.

m⁶A restoration rescues disease-related phenotypes

We next examined whether elevating the m⁶A level could rescue the disease-related phenotypes in *C9ORF72*-ALS/FTD patient iPSNs. We either overexpressed the METTL14 methyltransferase (Extended Data Fig. 10a) or knocked down the FTO demethylase (Extended Data Fig. 10b) via lentiviral transduction in neurons differentiated from patient iPSCs. Both approaches significantly increased the m⁶A level (Fig. 6a). Elevation of m⁶A on the hypomethylated mRNA transcripts reduced their abnormal upregulation in *C9ORF72* iPSNs (Fig. 6b,c), indicating the restoration of the RNA homeostasis in patient neurons. Furthermore, the m⁶A upregulation on the *C9ORF72* repeat-containing intron RNA (Fig. 6d) also effectively decreased the repeat RNA abundance, measured by both RT-qPCR of the intron region (Fig. 6e) and RNA fluorescence in situ hybridization (FISH) targeting the sense GGGGCC repeats (Fig. 6f). Accordingly, the endogenous poly-GP level was also reduced in patient iPSNs (Fig. 6g).

Additionally, we examined the antisense repeat-containing RNA, which is produced by bi-directional transcription at the repeat expansion region and could potentially contribute to the pathogenesis²⁶⁻³⁰. Using both RNA FISH and stranded RT-qPCR^{27,31}, we found that the antisense RNA, similar to the sense repeat-containing intron, was also reduced by METTL14 overexpression or FTO knockdown in patient iPSNs (Fig. 6h,i). Notably, the total *C9ORF72* mRNA level was not affected by m⁶A changes (Fig. 6j). This reveals the exciting opportunity to diminish both strands of the potentially toxic repeat RNAs and derived DPRs without influencing the *C9ORF72* protein expression by manipulating one candidate genetic modifier.

Finally, we tested whether increasing m⁶A can improve neuron survival. *C9ORF72*-ALS/FTD iPSNs are more susceptible to glutamate-induced excitotoxicity compared to controls³². We quantified the percentage of neuron death after glutamate treatment and found that either METTL14 overexpression or FTO knockdown was sufficient to alleviate the glutamate-induced cell death of *C9ORF72* iPSNs and largely improved neuron survival (Fig. 6k and Extended Data Fig. 10c,d). These results support the m⁶A pathway as a reversible target that could provide beneficial effects to *C9ORF72* repeat expansion-linked neurodegeneration.

FTO inhibitor treatment mitigates disease-linked phenotypes

Small molecule approaches to inhibit the demethylase activity is another way to elevate m⁶A levels. Several small molecule inhibitors of FTO have been developed and reported to exhibit anti-tumor efficacy³³⁻³⁵. In particular, CS2 is the latest generation of FTO inhibitor, which showed high potency on FTO inhibition and promising anti-cancer effect³⁴. Treatment of *C9ORF72*-ALS/FTD patient iPSNs with CS2 increased the total m⁶A level on mRNA (Fig. 7a), reduced repeat RNA and DPR levels (Fig. 7b,c), and significantly improved neuron survival (Fig. 7d). This highlights the therapeutic potential of targeting FTO in the neurodegeneration disease.

Discussion

Here, we found that the expression of the two m⁶A methyltransferases METTL3 and METTL14 is abnormally reduced, triggered by the repeat-containing RNA. On the one hand, the abnormal m⁶A reduction led to the transcriptome-wide mRNA dysregulation with significant enrichment in synaptic activity and neuronal functional pathways. On the other hand, the reduced m⁶A mark on the repeat-containing RNA disturbed the RNA decay, therefore enhancing the accumulation of toxic repeat RNA and DPRs, which further promote m⁶A dysregulation, forming a positive feedback loop. Strategies to elevate the m⁶A RNA modification level have the therapeutic potential in *C9ORF72*-ALS/FTD, as this can both reduce the toxic DPR/RNA repeats and rescue a broad spectrum of post-transcriptional dysregulation in patient neurons. Thus, this work provides evidence of m⁶A epitranscriptomic dysregulation as a previously unknown pathogenic mechanism of *C9ORF72*-ALS/FTD (Fig. 7e)

The nervous system has extremely complex RNA processing regulation, including alternative splicing, polyadenylation, transport, stability and translation. Epitranscriptomic

regulation recently emerges to play important roles in modulating the functions and structures of RNAs in a spatiotemporal manner and therefore fine-tuning the accuracy of gene expression³⁶. Several studies demonstrated the important roles of m⁶A in regulating brain function. Loss of m⁶A methyltransferases in *Drosophila* leads to severe locomotion defects in orientation, walking speed and activity due to impaired neuronal function³⁷. Mice with m⁶A pathway loss-of-function displayed multiple brain defects, including smaller brains, weakened spatial learning and memory, and impaired synaptic transmission, long-term potentiation and axon regeneration^{17,38}. This suggests the importance of the m⁶A-mediated epitranscriptome in neural function, but there were limited studies on its contribution to human neurological or neurodegenerative diseases.

We found that the global m⁶A reduction leads to transcriptome-wide hypomethylation and dysregulated gene expression in C9ORF72-ALS/FTD patients. The hypomethylated genes in C9ORF72-ALS/FTD are enriched in neuronal functions and synaptic pathways. In particular, many genes are linked to glutamatergic synapses and calcium signaling pathways. This could potentially contribute to the underlying molecular mechanism of hyperexcitability and increased vulnerability to excitotoxicity of patient neurons^{32,39,40}. Indeed, METTL14 deletion has been found to result in increased neuronal excitability in striatonigral neurons, through lowered current threshold of action potential generation⁴¹.

There are several hypotheses of the molecular mechanisms on how C9ORF72 repeat expansion leads to neurodegeneration. The haploinsufficiency of the C9ORF72 protein function might contribute to the disease progression, especially via microglia-mediated deficits^{42,43}. But more evidence points to the driving toxicity from the abnormally accumulated sense or/and antisense repeat RNAs, and their encoded DPRs. We now identified that both strands of repeat-containing RNAs can be regulated by the m⁶A-mediated RNA degradation. Elevating the m⁶A level (such as by expressing the methyltransferase METTL14 or by reducing the demethylase FTO) can directly decrease the RNA repeats of both strands, the major upstream toxicity-initiating factors, therefore rescue the overall downstream defects and improve neuronal health. Importantly, the *C9ORF72* mRNA level was not affected by m⁶A, thus the normal protein function will not be affected by this strategy. Furthermore, as the m⁶A RNA modification is decreased in patients, this approach will restore the m⁶A level and rescue the global hypomethylation-mediated dysfunction of essential neuronal genes. All these advantages support the premise of targeting the m⁶A pathway as a novel therapeutic strategy in C9ORF72-ALS/FTD. It will be interesting to test the rescue efficacy *in vivo* using appropriate C9 mouse models in future studies.

It is also noteworthy that the overexpression of the C9 expanded repeats, rather than the DPRs produced by randomized codons, induced METTL3/14 expression decrease. Although the mechanism by which the repeat expansion elicited reduction of METTL3/14 expression remains to be determined, our data emphasize the role of repeat expansion-mediated RNA toxicity in disease-related neuronal deficits. Many recent studies focused on various mechanisms of DPR-mediated neurotoxicity⁴⁴. The repeat RNA-induced toxicity could also play important roles in disease pathogenesis. It is generally believed that the repeat RNA could sequester specific RBPs from their normal targets, therefore perturb their

physiological functions. Multiple RBPs have been proposed to be bound and disturbed by the (GGGGCC)_n repeat RNA^{45,46}, such as ADARB2³², hnRNPs⁴⁷⁻⁴⁹, and Pur-α^{49,50}. However, the pathophysiological contribution of many candidate RBPs remains elusive. Our study reveals a novel mechanism of repeat RNA-mediated toxicity - disturbing the global RNA stability homeostasis via m⁶A modification. Besides the effect on mRNAs, the m⁶A reduction also leads to stabilization of repeat-containing intron RNA, which provides translation substrate for increased production of DPRs. Therefore, this repeat RNA toxicity mechanism might be an early event that can be targeted to reduce both RNA and DPR mediated downstream defects.

In addition, it is noted that the core components of the m⁶A writer complex are also widely reduced in sporadic ALS from analysis of almost one hundred sporadic ALS iPSN lines and seven postmortem tissues (Extended Data Fig. 3). This implicates the possible broader contribution of the m⁶A-mediated RNA dysregulation in sporadic ALS as well. A recent study reported m⁶A hypermethylation in spinal cord of four sporadic ALS patients using a microarray method⁵¹. Considering the complexity of sporadic disease, screening m⁶A levels in a large number of sporadic ALS cases by using direct UHPLC-QQQ-MS/MS may be necessary. Future development of new techniques to reveal spatial or single-cell m⁶A changes will also help elucidate m⁶A dysregulation in diseases with heterogeneous pathology. Interestingly, the m⁶A pathway was also implicated in other neurodegenerative diseases. METTL3/14 expression and the m⁶A level has been reported to be reduced in the neurons or brains of Alzheimer's Disease (AD) patients^{52,53}, 5×FAD mouse model⁵⁴, and 6-OHDA induced rat model of Parkinson's Disease⁵⁵. A recent study reported that treating primary neurons with Aβ oligomers causes reduced METTL3 expression⁵². Although the molecular mechanisms of the m⁶A dysregulation remain elusive, these studies suggest the epitranscriptome dysregulation as a compelling convergent pathogenic pathway underlying neurodegenerative diseases. Further work is needed to elucidate the mechanisms how the expression of m⁶A writer or eraser proteins is altered, which could provide more therapeutic options to rescue the epitranscriptome deficits in neurodegeneration. Overall, our study highlights the significance of understanding RNA modification-mediated pathogenic mechanism and opens new avenues of developing novel epitranscriptomic therapy in neurodegenerative diseases.

Methods

Plasmids

To delete the intron sequences upstream of the GGGGCC repeats, we used HindIII and BssHII to cut out the upstream intron sequences in the monocistronic C9R-NLuc luciferase reporters for (GGGGCC)₇₀ RAN translation^{5,22}. For the lentiviral C9R-NLuc reporters, the (GGGGCC)₇₀-NLuc fragments from the monocistronic mRNA luciferase reporters were cut out by PmeI and XhoI, and subcloned into the lentiviral vector under the EF1a promoter via SbfI (blunted by NEB Quick Blunting Kit) and XhoI. For lentiviral METTL14 overexpression, the Flag-METTL14 fragment was cut out by EcoRI and BamHI from the pcDNA3-Flag-METTL14 (Addgene# 53740), and subcloned into the lentiviral vector under the EF1a promoter via the same restrictive enzyme sites. For the design and cloning of

lentiviral *METTL14* and *ZCCHC8* shRNAs, we followed the Addgene pLKO.1 shRNA cloning protocol (<https://www.addgene.org/protocols/plko/>). In brief, oligos containing the targeting sequences of each gene (listed below) were annealed and ligated to the pLKO.1 cloning vector via AgeI and EcoRI sites. For lentiviral 160× GGGGCC repeat expression, the fragment of 80× GGGGCC was cut out from the pcDNA5-FRT-TO-(GGGGCC)₈₀-NLuc by KpnI and SmaI, and cloned back via the KpnI and BssHII (blunt) sites upstream of the (GGGGCC)₈₀ in the original pcDNA5-FRT-TO-(GGGGCC)₈₀-NLuc plasmid in order to expand the repeat length to 160× GGGGCC repeats. Next, the fragment containing 160× GGGGCC repeat was cut out by KpnI and SmaI, and subcloned into the lentiviral vector under the EF1a promoter via KpnI and NheI (blunt). For the lentiviral plasmids expressing poly-GA or poly-GR with randomized codons, the sequences encoding the randomized 50×GA or 50×GR with ATG start codon were synthesized (Genewiz) and inserted in the lentiviral vector under the EF1a promoter with 2×FLAG at the 3' end. The HiBiT tag was linked to the 5' of APEX2 by PCR amplification from APEX2-OMM (Addgene #79056), and inserted upstream of GFP/GA50/GR50 at the XbaI and BamHI sites.

Cell culture and transfection

Control and patient lymphoblast cells were maintained as described²³ (Supplementary Table 1): cells were grown in RPMI1640 supplemented with 10% (v/v) FBS, 2mM L-Glutamine, 100 µg/ml streptomycin and 100 U/ml penicillin. HeLa Flp-In dual luciferase reporter cells^{5,22,23} and 293T cells were grown in DMEM supplemented with 10% (v/v) FBS, 100 µg/ml streptomycin and 100 U/ml penicillin. 293T cells were used for the lentivirus packaging. All cells were maintained at 37°C with 5% CO₂.

Lipofectamine RNAiMAX (Thermo Fisher Scientific) was used to transfect siRNAs following the manufacturer's protocol. The siRNAs targeting *METTL14* (Cat# M-005170-01), *ZCCHC8* (M-021026-00), and the Non-Targeting control were purchased from GE Dharmacon. Single siRNAs were used to knock down YTHDC1 (targeting sequence: 5'-GTCGACCAGAAGATTATGATA-3') and YTHDF2 (targeting sequence: 5'-AAGGACGTTCCCAATAGCCAA-3') as previously described^{9,15}. 293T cells were used to package lentivirus expressing non-targeting control shRNA (Addgene #10879), YTHDC1 shRNA (Sigma, #TRCN0000243989), *ZCCHC8* shRNA (targeting sequence: 5'-TTAGCACTGAGAGCTATTAA-3'), FTO shRNA (Sigma, #TRCN0000246247), *METTL14* shRNA (targeting sequence: 5'-CCATGTACTTACAAGCCGATA-3'), and lentiviral *METTL14* overexpression plasmid. Three biological replicates were prepared at each condition for RNA quantification and luciferase reporter experiments. The NLuc luciferase activity was measured by Nano-Glo Dual Luciferase Assay (Promega) on Tecan Infinite 200 PRO. NLuc levels were normalized to total protein amounts for each sample. Protein lysates were quantified by BCA Assay (ThermoFisher Scientific).

Human iPSC and iPSC-derived neurons

C9ORF72-ALS/FTD and non-neurological control iPSC lines were obtained from the Answer ALS repository at Cedars-Sinai iPSC Core (see Supplementary Table 2 for demographics). Presence or absence of the C9ORF72 repeat expansion was verified by repeat-primed PCR (RP-PCR)⁵⁶. iPSCs and iPS-neurons were routinely checked for

the expression of poly(GP) level. iPSCs were maintained in mTeSR media on growth factor reduced Matrigel (Corning, Cat# 354230), following the Cedars-Sinai Standard Operating Procedure (SOP, <https://www.cedars-sinai.edu/content/dam/cedars-sinai/research/documents/biomanufacturing/complete-ipsc-culturing-protocol-rev-4-2020.pdf>). iPSCs were differentiated into spinal neurons using the direct induced motor neuron protocol as described⁵. The i³Neuron iPSC line¹⁹ was obtained from Dr. Michael Ward's lab. The i³Neuron iPSCs were cultured in Essential 8 media (Thermo Fisher Scientific) on Matrigel (Corning, Cat# 354277), differentiated into i³Neuron using the protocol as described¹⁹, and harvested on Differentiation Day 14. All cells were maintained at 37°C with 5% CO₂.

To overexpress METTL14 or knock down FTO in C9ORF72-ALS/FTD iPSNs, neurons were transduced with lentivirus expressing GFP or METTL14, or control shRNA or FTO shRNA on Day 18 post-differentiation, and then harvested 7 days after infection for protein and RNA assays, or maintained till Day-32 differentiation for glutamate-induced excitotoxicity assay. The FTO inhibitor CS2 (also named brequinar, Cayman Chemical, Cat# 24445) was added at 500nM on Day 16 post-differentiation, and the neurons were harvested after 7 days for protein and RNA assays. For glutamate-induced excitotoxicity assay, CS2 (500nM) was added on differentiation day 25 and the assay was performed on day 32. Neurons were fed with fresh media with CS2 every other day. To harvest relatively pure neuron population for protein and RNA assays from the iPSN culture, iPSNs were gently washed once with 1×PBS, and then collected by using 1×PBS to wash off the neuron matrix followed by bench-top spin and 1×PBS wash.

For glutamate-induced excitotoxicity of patient iPSNs, neurons were treated with 0 or 10μM L-glutamate for 4 hours on day 32 of differentiation. After 3.5 hours, the cells were stained with Hoechst33342 (5μg/ml) and Propidium Iodide (1μg/ml) for 30 min to visualize total and dead cells under ZEISS Axio Observer^{57,58}. Images were taken randomly. At least 350 neurons were quantified per replicate blindly.

For expressing 160× GGGGCC repeat or poly-GA/GR with randomized codons using i³Neurons, cells were transduced with lentivirus expressing the different transgenes on differentiation day 5 at an MOI of 1.5 in Cortical Neuron Culture Medium¹⁹, and harvested on differentiation day 14 for the measurement of endogenous *METTL3* and *METTL14* expression. The expression of poly-DPR constructs post transduction was measured via the Nano-Glo HiBiT Lytic Detection System (Promega, Cat# N3030), and visualized by immunofluorescent with the FLAG antibody (Sigma, F1804, 1:500).

For luciferase assays using i³Neurons, cells were first transduced with lentivirus expressing luciferase reporters on differentiation day 2 at an MOI of 1 in Cortical Neuron Culture Medium¹⁹. On differentiation day 5, the cells were transduced with lentivirus expressing non-targeting control shRNA, METTL14 shRNA, YTHDC1 shRNA or ZCCHC8 shRNA. Semi-media change was performed every other day till the harvest day. i³Neurons were harvested on differentiation day 14 for luciferase and RNA assays.

For all assays, the cells were plated randomly in multiple-well plates and were randomly assigned to different experiment groups.

Human tissue and immunohistochemistry

C9ORF72-ALS/FTD patient and non-neurological control postmortem brain tissues and paraffin-embedded temporal cortex sections were obtained from Johns Hopkins ALS Postmortem Tissue Core and Target ALS Postmortem Tissue Core with approval from patient consent (see Supplementary Table 3 and 4 for demographic information). The study using patient samples/data was approved by the Johns Hopkins University School of Medicine Office of Human Subjects Research Institutional Review Boards. Tissue sections were gradually rehydrated with xylene twice for 10 min, 100% ethanol twice for 10 min, 95% ethanol twice for 5 min, 70% ethanol for 5 min, 50% ethanol for 5 min, 30% ethanol for 5 min, PBS for 5 min and finally dH₂O for 5 min. Antigen retrieval was performed with 0.1M sodium citrate buffer (pH 6.0) for 5min in a steam sterilizer. The slides were permeabilized with 0.2% Triton X-100 for 20min and blocked with the blocking buffer (1% BSA and 2% Goat Serum diluted in 1× PBS) for 1 hour. Slides were incubated in each primary antibody diluted in the blocking buffer overnight at 4°C. On the next day, slides were washed three times for 5 min with 1× PBS, and treated with 0.3% H₂O₂ for 30min. After incubation with secondary antibody (Goat Anti-Rabbit IgG (H+L), Biotinylated, Vector Laboratories BA-1000-1.5, 1:300) for 1 hour, the slides were treated with the R.T.U. VECTASTAIN Elite ABC Reagent for 30min. Finally, the slides were developed using the DAB Peroxidase Substrate Kit (Vector Laboratories SK-4100) for exactly 1 minute each. Slides stained with METTL14 were also counterstained before mounting. Slides were imaged with Keyence BZ-X all-in-one fluorescent microscope. All images were acquired using identical exposure time and conditions. Primary antibodies: METTL14 (Sigma-Aldrich HPA038002, 1:500), METTL3 (Abcam ab195352, 1:500), YTHDC1 (Sigma-Aldrich HPA036462, 1:500), YTHDF2 (Abcam ab246514, 1:2500).

Immunoblotting

Samples were homogenized in RIPA buffer supplemented with 1× cOmplete protease inhibitor cocktail (Sigma). Homogenates were spun at 21,130g for 10 min at 4°C. The protein concentrations of supernatants were determined using BCA protein assay (Thermo Fisher Scientific 23224). Equal amount of protein samples was loaded on 10% acrylamide gel and transferred to nitrocellulose membrane (GE Healthcare). Membrane was blocked in 5% non-fat milk/TBST for 30-60 min at room temperature and incubated with primary antibody (1:1000) overnight at 4 °C. After TBST wash, the membrane was incubated with HRP-linked secondary antibody (Cytiva, 1:10,000) for 1 hour. Protein bands were detected using Clarity Western ECL Substrate kit (Bio-Rad) or SuperSignal West Pico PLUS Chemiluminescent Substrate kit (Thermo Fisher Scientific) and imaged using a ChemiDoc Imager (Bio-Rad). Analysis was conducted using Fiji. Inter-group differences were assessed by two-tailed Student's *t*-test. Primary antibodies: METTL14 (Sigma-Aldrich HPA038002), METTL3 (Abcam ab195352), YTHDC1 (Sigma-Aldrich HPA036462), YTHDF2 (Abcam ab220163) and ZCCHC8 (Proteintech 23374-1-AP).

RNA isolation and RT-qPCR

Total RNAs were isolated with TRIZOL reagent (Invitrogen). RNA samples used for RT-qPCR were treated with RQ1 DNase I (Promega) and then used for complementary

DNA (cDNA) synthesis with random hexamers (Thermo Fisher Scientific). qPCR was performed using SYBR Green Master Mix (Thermo Fisher Scientific) on the CFX96 real-time PCR detection system (Bio-Rad). The *C9ORF72* repeat-containing intron RNA levels in patient samples were measured using TaqMan fast advanced master mix (Thermo Fisher Scientific). For the quantification of antisense repeat RNA levels³¹, the reverse transcription was performed using the antisense strand-specific primer (Supplementary Table 5) via the Superscript III reverse transcriptase (Thermo Fisher Scientific), and then subjected to qPCR using TaqMan fast advanced master mix. Custom primer sequences are listed in Supplementary Table 5. Human ACTB primer set (Hs.PT.56a.40703009.g) was purchased from Integrated DNA technologies. At least three biological replicates with each containing two technical replicates were used for quantification. *GAPDH* or *HPRT1* mRNA was used as the internal control. Inter-group differences were assessed by two-tailed Student's *t*-test.

LC-MS/MS quantification of m⁶A in RNA

Non-ribosomal RNA was extracted from the total RNA using the RiboMinus transcriptome isolation kit (Thermo Fisher Scientific) following the manufacturer's protocols. Polyadenylated RNA (poly-A RNA) was purified using NEBNext Poly(A) mRNA Magnetic Isolation Module (New England Biolabs). 50 ng of poly-A RNA or non-ribosomal RNA was digested with 1U nuclease P1 in 30μl of buffer containing 20 mM of NH₄OAc for 2 h at 42 °C. 1× FastAP Buffer and 1U FastAP Thermosensitive Alkaline Phosphatase (Life Technology) were added to the samples. The reaction was carried out at 37 °C for an additional 2 hours, and then centrifuged through filters (0.22 μm pore size, 4 mm diameter, Millipore). Nucleosides in the filtered samples were separated by reverse phase ultra-performance liquid chromatography (C18 column) and detected by Triple Quad 6500 System (AB SCIEX) in a positive ionization mode. The nucleosides were quantified by using the nucleoside-to-base ion mass transitions of 282 to 150 (m⁶A), and 268 to 136 (A). A standard curve was obtained from pure nucleoside standards in the same batch of samples. The m⁶A/A ratio was calculated based on the calibrated concentrations comparing to the standard curve.

Immunoprecipitation

One 10cm dish of neurons per line were harvested on day 18 of differentiation and washed two times with cold PBS. After centrifugation at 211g for 5min, the neuron pallet was lysed in 400μl lysis buffer, composed of 20mM Tris pH7.4, 200mM NaCl, 0.5% NP-40, 1mM DTT, 0.1mM EDTA, 0.1mM EGTA, 1× cOmplete protease inhibitor cocktail (Sigma) and SUPERase-in RNase Inhibitor (0.25μl/100μl, Thermo Fisher Scientific). The lysate was sheared with 26-gauge needle for 6 times, incubated on ice for 5min, and subsequently centrifuged at 21,130g for 20min at 4. Protein G Dynabeads were washed once with PBST (PBS with 0.02% Tween-20) and incubated with YTHDC1 antibody (Sigma-Aldrich HPA036462) or rabbit IgG (Sigma) four-volume of wash buffer with rotation for 1 hour at RT. The antibody-coated beads were washed three times with lysis buffer and incubated with the supernatant of the cell lysates at 4 °C for 1 hour with rotation. After the incubation, the beads were wash five times with lysis buffer. The proteins bound on the beads were eluted in SDS loading buffer and heated at 95°C for 5min.

MeRIP-seq and MeRIP-RT-qPCR

Ribosomal RNA was depleted from total RNA by RiboMinus Eukaryote Kit v2 (Thermo Fisher Scientific). m⁶A-immunoprecipitation (m⁶A-IP) was performed using the EpiMark N6-Methyladenosine Enrichment Kit (New England Biolabs) following the manufacturer's protocols. Library preparation was performed using the SMARTer Stranded Total RNA-Seq Kit v2 (Takara). Sequencing was performed at the University of Chicago Genomics Facility on an Illumina NovaSeq 6000 system for paired-end 50bp. For MeRIP-RT-qPCR, the m⁶A-modified *GLuc* RNA (NEB) was spiked in as the reference control before the m⁶A-immunoprecipitation. RNAs were extracted from m⁶A-IP and input fractions, and subjected to reverse transcription and qPCR. The *GLuc* RNA was used as normalization control. The fold enrichment of m⁶A-IP was compared to the input. Inter-group differences were assessed by two-tailed Student's *t*-test. Rabbit IgG antibody was used as the negative control.

YTHDF2 RNA immunoprecipitation (RIP)-seq

The iPSNs were harvested on day 22 of differentiation. The cell pallets were resuspended in equal volume of RIP lysis buffer (50mM HEPES, 150mM KCl, 2mM EDTA, 0.5% NP40, 0.5mM DTT, supplemented with 1× cOmplete protease inhibitor cocktail (Sigma), 0.25μl/100μl SUPERase-in RNase Inhibitor (Thermo Fisher Scientific)). The lysates were sheared with 26-gauge needle for 6 times, lysed on ice for 5min and centrifuged at 14,000g for 30min at 4 °C. Protein A/G beads (Thermo Fisher Scientific) were washed once with RIP lysis buffer, and incubated with YTHDF2 (Abcam ab246514) or rabbit IgG antibody (Sigma) for 1 hour at 4 °C. The antibody-coated beads were washed two times with RIP lysis buffer. The supernatants of the lysates were added to the pre-cleared beads and rotate at 4 °C for 4 hours. 5% of the lysates was saved as input and mixed with 1ml TRIZOL for RNA extraction. The beads were washed 6 times with NT2 buffer (50mM HEPES, 200mM NaCl, 2mM EDTA, 0.05% NP40, 0.5mM DTT, protease inhibitor and RNase inhibitor). After washing, 1ml TRIZOL was added to the beads to elute the RNA. RNAs recovered from RIP and input were subjected to NEBNext Ultra II Directional RNA Library Prep (New England Biolabs) coupled with NEBNext Poly(A) mRNA Magnetic Isolation Module (New England Biolabs).

Meso Scale Discovery (MSD) ELISA

The endogenous GP level from iPSNs was quantified as previously described⁵. Briefly, the streptavidin coated plates were blocked in 1% blocker A in PBS (all reagents from MSD) overnight at 4 °C and coated with 0.375 μg/mL biotinylated rabbit anti-GP antibody. 35 μl of cell lysates was added in duplicate, along with a standard curve of GP8 peptide. Following a 3-hour incubation at room temperature, wells were washed with PBST, and sulfo-tagged detection antibody (0.5 μg/mL) was added. After incubation and washes, read buffer was added followed by immediate imaging using MESO QuickPlex SQ 120.

RNA fluorescent in situ hybridization (FISH)

LNA-incorporated DNA probes with TYE-488 dye (Exiqon) were used against the (GGGGCC)_n RNA repeats or (CCCCGG)_n RNA repeats²⁷. Cells growing on coated

coverslips were fixed with 4% PFA at room temperature for 15min and permeabilized with 0.25% Triton X-100 in PBS for 15 min. The cells were incubated with the pre-hybridization buffer (10% Dextran Sulfate, 10% deionized formamide in 2× SSC supplemented with 0.1mg/mL E.coli tRNA, 10mM Ribonucleoside Vanadyl Complex (NEB #S1402S), and SUPERaseIn RNase inhibitor (Ambion)) at room temperature for 30 min. The FISH probes for sense repeats and antisense repeats were diluted to 50 nM in the hybridization buffer and incubated with the cells at 60 °C for 3 hours, followed by two washes with 10% formamide in 2× SSC at 60 °C for 10 min each and three washes with 2× SSC at room temperature. Cells were then stained with DAPI and mounted for imaging. FIJI was used to quantify RNA foci.

Proteomic data analysis

Proteomic data matrix was downloaded from NeuroLINC and Answer ALS databases (see Supplementary Table 6 for demographics). Proteins with absent values in more than 4 samples were removed from the list. For Answer ALS data, protein expression among each batch was normalized using the value of the corresponding AE8 iPSN batch control. Z-score was calculated for each protein between the control and patient samples of NeuroLINC or AnswerALS. Wilcox test was used to determine significance.

RNA decay measurement

5 µg/ml Actinomycin D was added to HeLa Flp-In dual luciferase reporter cells or day-32 iPSNs at 6 h, 3 h, and 0 h before collection for RNA extraction by Trizol. For RNA-seq, same proportion of ERCC RNA spike-in control (Ambion) was added to each sample before poly-A selection. Library preparation was performed using NEBNext Ultra II Directional RNA Library Prep (New England Biolabs) coupled with NEBNext Poly(A) mRNA Magnetic Isolation Module (New England Biolabs). To measure the half-life of *C9ORF72* repeat RNA, equal amount of *CLuc* RNA (New England Biolabs) was spiked in before reverse transcription as normalization control for qPCR. Sequencing was performed on a NovaSeq platform for paired-end 150bp.

m⁶A-seq analysis

Raw reads were trimmed with Trimmomatic-0.39⁵⁹, then aligned to human genome and transcriptome (hg38) using HISAT (version 2.1.0)⁶⁰ with ‘--rna-strandness RF’ parameters. Annotation files (version v29, 2018-08-30, in gtf format) were downloaded from GENCODE database (<https://www.genencodegenes.org/>). Mapped reads were separated by strands with samtools (version 1.9)⁶¹ and m⁶A peaks on each strand were called using MACS (version 2)⁶² with parameter ‘-nomodel, --keep-dup 5, -g 2.052e9, --tsize 60 -extsize 150’ separately. Peaks with $q < 0.01$ were considered as significant ones. Significant peaks identified in at least three biological replicates were merged using bedtools (v.2.26.0)⁶¹ and were used in the subsequent analysis. Differentially methylated peaks were called with MeTDiff⁶³ with default parameters.

RNA-seq analysis

Raw reads were trimmed with Trimmomatic-0.39⁵⁹, then aligned to human genome and transcriptome (hg38) using HISAT (version 2.1.0)⁶⁰ with ‘--rna-strandness RF’ parameters. Annotation files (version v29, 2018-08-30, in gtf format) were downloaded from GENCODE database (<https://www.genencodegenes.org/>). Reads on each GENCODE annotated gene were counted using HTSeq⁶⁴ and then differentially expressed genes were called using DESeq2 package in R⁶⁵ requiring at least 10 read counts in at least three samples with p value < 0.05.

RNA half-life analysis

Raw reads were trimmed with Trimmomatic-0.39⁵⁹, then aligned to human genome and transcriptome (hg38) and external RNA Control Consortium (ERCC) RNA spike-in control (Thermo Fisher Scientific) using HISAT (version 2.1.0)⁶⁰ with ‘--rna-strandness RF’ parameters. Annotation files (version v29, 2018-08-30, in gtf format) were downloaded from GENCODE database (<https://www.genencodegenes.org/>). Reads on each GENCODE annotated gene were counted using HTSeq⁶⁴ and then normalized to counts per million (CPM) using edgeR⁶⁶ packages in R. CPM was converted to attomole by linear fitting of the RNA ERCC spike-in. Half-life of RNA was estimated using formula listed in the previous publication²⁴. Specifically, as actinomycin D treatment results in transcription stalling, the change of RNA concentration at a given time (dC/dt) is proportional to the constant of RNA decay (K_{decay}) and the RNA concentration (C), leading to the following equation:

$$\frac{dC}{dt} = -K_{decay}C$$

Thus, the RNA degradation rate K_{decay} was estimated by:

$$\ln\left(\frac{C}{C_0}\right) = -K_{decay}t$$

To calculate the RNA half-life ($t_{1/2}$), when 50% of the RNA is decayed (that is, $\frac{C}{C_0} = \frac{1}{2}$), the equation was:

$$\ln\left(\frac{1}{2}\right) = -K_{decay}t_{1/2}$$

From where:

$$t_{1/2} = \frac{\ln 2}{K_{decay}}$$

The final half-life was calculated by using the average value of 0 h, 3 h and 6 h.

YTHDF2 RIP-seq analysis

Raw reads were trimmed with Trimmomatic-0.39⁵⁹, then aligned to human genome and transcriptome (hg38) using HISAT (version 2.1.0)⁶⁰ with '--rna-strandness RF' parameters. Annotation files (version v29, 2018-08-30, in gtf format) were downloaded from GENCODE database (<https://www.gencodegenes.org/>). Reads on each GENCODE annotated gene were counted using HTSeq⁶⁴ and then differentially expressed genes were called using DESeq2 package in R⁶⁵. Differentially upregulated genes requiring at least 10 read counts in at least three samples with p adjusted < 0.05 were identified as YTHDF2 target genes.

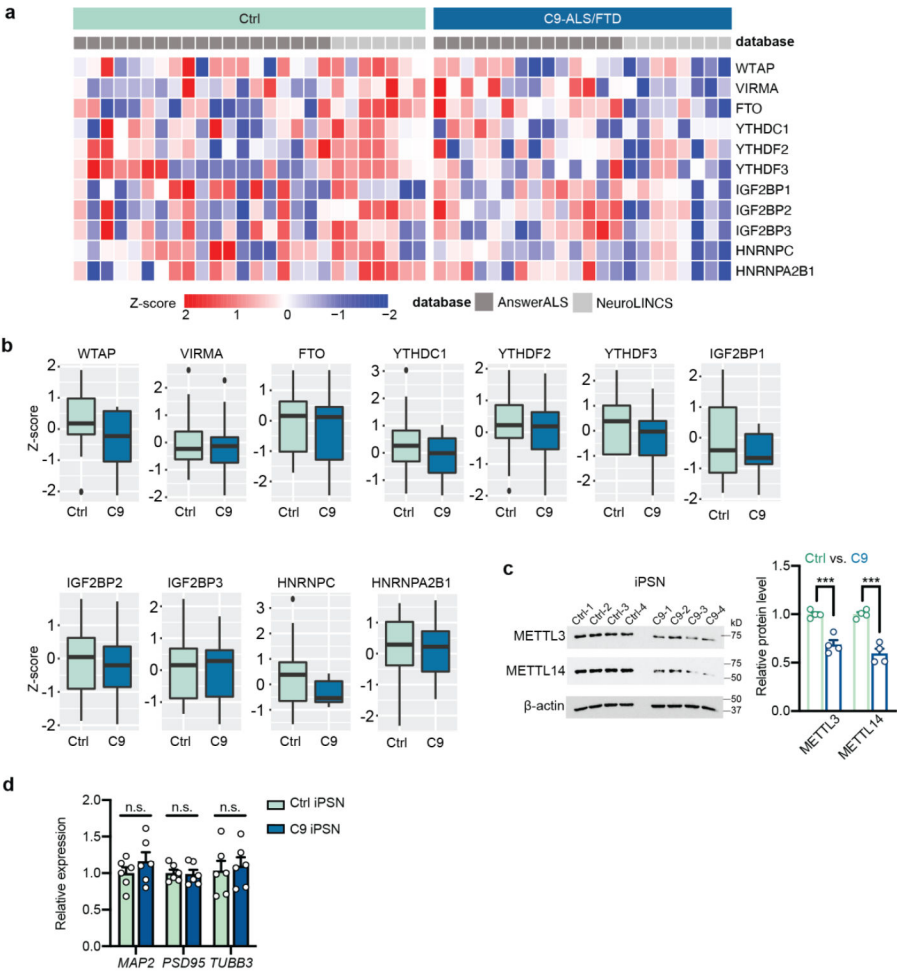
Enrichment analysis

Motif enrichment analysis was performed with HOMER (version 4.11)⁶⁷ in RNA mode, and GO enrichment analysis was performed with DAVID (version 6.8)⁶⁸⁻⁷⁰ with default parameter.

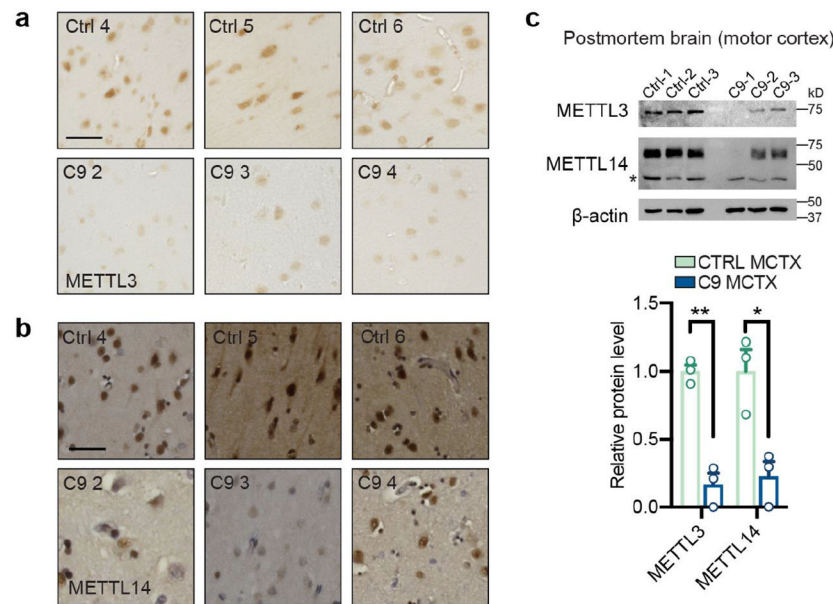
Statistics and reproducibility

Data shown were from at least three independent biological replicates or individual control or patient cell lines/tissue samples. Quantitative data were presented as mean with standard error of the mean (SEM). R or Prism (GraphPad Software) were used for statistical analysis, including Student's t-test, one-way ANOVA with multiple testing, non-parametric Wilcoxon-Mann-Whitney test, Fisher's exact test where appropriate. Statistical significance defined as $p < 0.05$ (*), $p < 0.01$ (**), $p < 0.001$ (***), and $p < 0.0001$ (****). Statistical details of experiments can be found in the figure legends. No statistical methods were used to pre-determine sample sizes but our sample sizes are similar to those reported in previous publications^{5,22,23,24}.

Extended Data

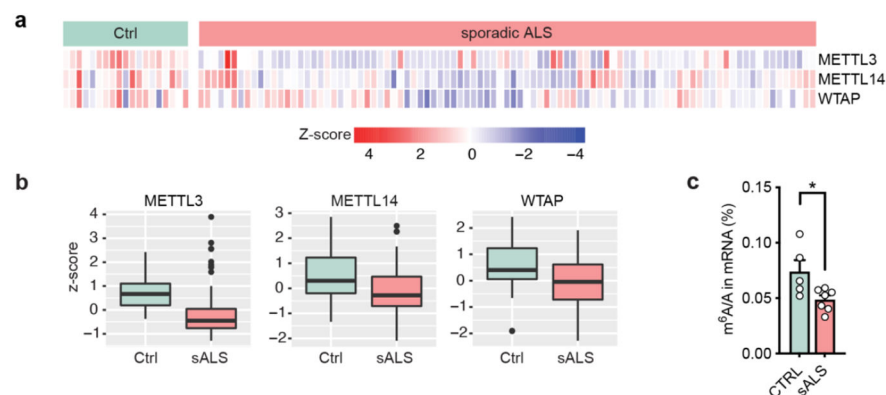


Extended Data Fig. 1: m⁶A pathway-related gene expression in C9ORF72-ALS/FTD iPSNs.
a, Proteomic heatmap of the m⁶A pathway components in control (n=26) and C9ORF72-ALS/FTD (n=22) iPSNs. Data were normalized to the batch controls. **b**, Boxplots of the proteomic data in (a). Box plots indicate the interquartile range with the central line representing the median, and the vertical lines extend to the extreme values in the group. **c**, Western blotting (left) and quantification (right) of METTL3 and METTL14 expression in control and C9ORF72 iPSNs. Data are mean \pm s.e.m. *** $p=0.0008$ and 0.0003 , respectively, by two-tailed t test. **d**, Relative RNA expression of neuronal marker genes (*MAP2*, *PSD95* and *TUBB3*) was measured by RT-qPCR in control and C9 iPSNs, showing comparable neuron maturity between control and C9. Points represent individual control or patient lines. $n=6$ in each group. Data are mean \pm s.e.m. *MAP2*: $p=0.304$; *PSD95*: $p=0.86$; *TUBB3*: $p=0.716$, by two-tailed t test.



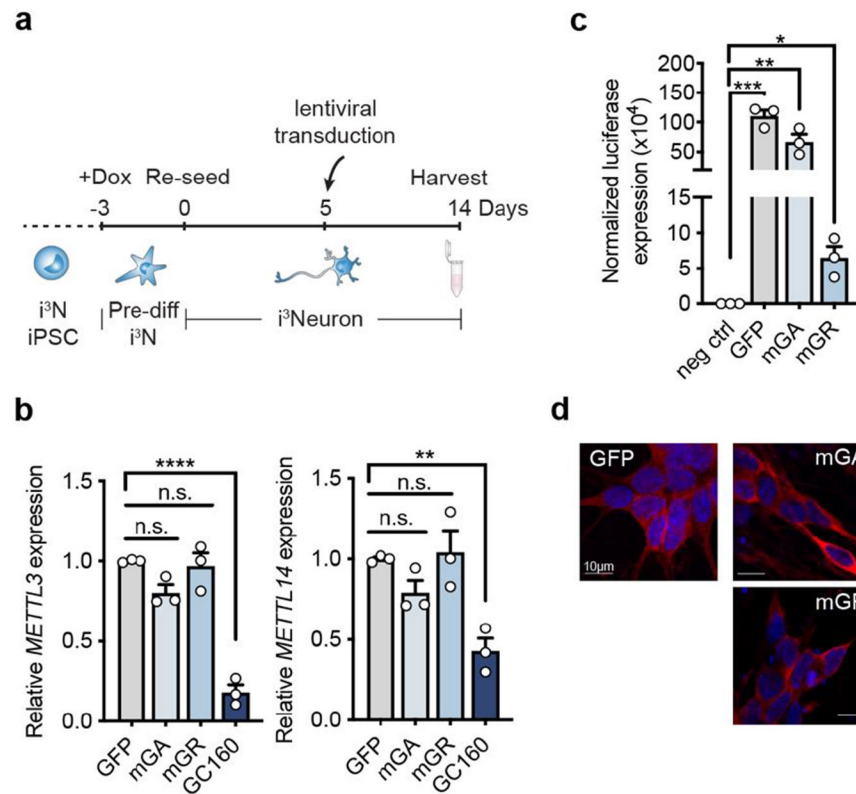
Extended Data Fig. 2: METTL3 and METTL14 m⁶A methyltransferases were reduced in C9ORF72-ALS/FTD postmortem brain.

a,b, Immunohistochemistry (IHC) staining of METTL3 (**a**), METTL14 (**b**) at temporal cortex section of control and C9ORF72-ALS/FTD samples. Scale bar = 50μm. **c**, Western blotting (top) and quantification (bottom) of METTL3, METTL14 using postmortem motor cortex tissue samples. *Non-specific bands. Points represent individual control or patient samples. n=3 in each group. Data are mean ± s.e.m. * $p=0.0171$, ** $p=0.0011$, by two-tailed t test.



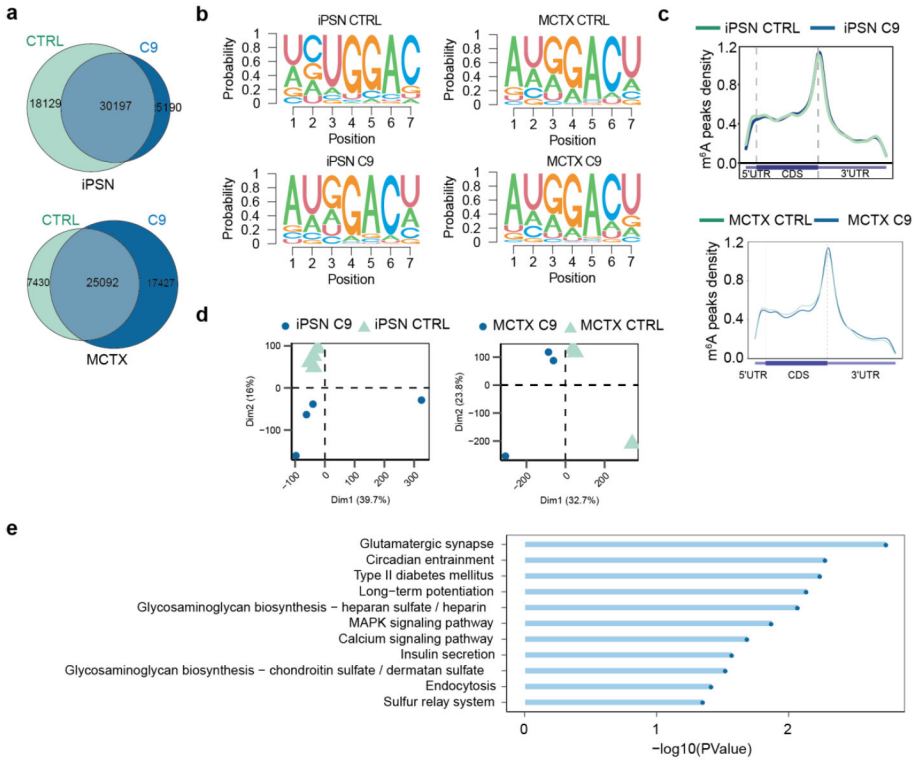
Extended Data Fig. 3: Expression changes of the m⁶A "writer" core components in sporadic ALS iPSNs.

a, Proteomic heatmap of the core components of m⁶A "writer" complex in control (n=19) and sporadic ALS (n=93) iPSNs. Data were normalized to the batch controls. **b**, Boxplots of the proteomic data in (**a**). Box plots indicate the interquartile range with the central line representing the median, and the vertical lines extend to the extreme values in the group. **c**, UHPLC-QQQ-MS/MS quantification of the m⁶A/A ratio in poly-A mRNAs from control (n=5) and sporadic ALS patient (n=7) postmortem frontal cortex. Data are mean ± s.e.m. Points represent individual samples. * $p=0.0247$ by two-tailed t test.



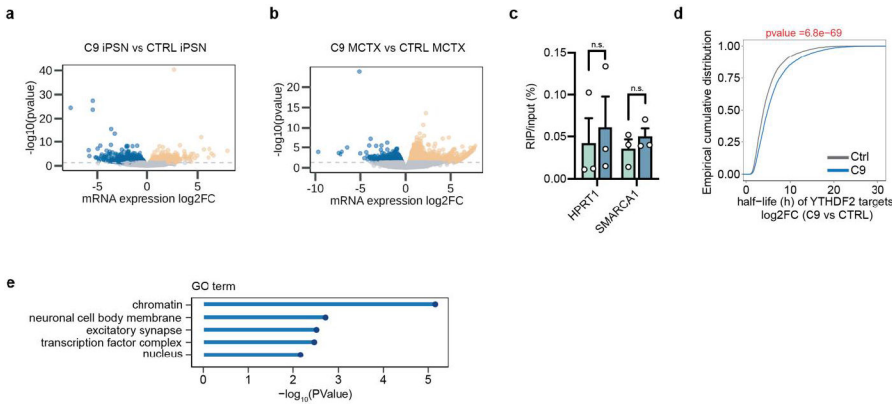
Extended Data Fig. 4: The repeat RNA induces downregulation of METTL3 and METTL14 expression.

a, Timeline for doxycycline-induced neuron differentiation, lentiviral transduction of transgenes to express repeats or DPRs, and functional analysis of i^3 Neurons. **b**, Relative RNA expression of *METTL3* and *METTL14* in i^3 Neurons expressing GFP control, modified poly-GA, modified poly-GR (with randomized codons), or (GGGGCC)₁₆₀ repeats. *METTL3*: mGA, $p=0.1154$; mGR, $p=0.9755$; GC160, **** $p<0.0001$. *METTL14*: mGA, $p=0.3892$; mGR, $p=0.9853$; GC160/GFP, ** $P=0.0073$. p-values were calculated by one-way analysis of variance (ANOVA) with Tukey's multiple comparisons. **c**, Detection of GFP, modified poly-GA and modified poly-GR post lentiviral transduction in i^3 Neurons by Nano-Glo HiBiT bioluminescence measurement. The luciferase signal was normalized to the total protein level. i^3 Neurons without lentiviral infection served as the negative control. * $p=0.0148$, ** $p=0.0062$, *** $p=0.0004$, by two-tailed t test. **d**, Immunofluorescent staining of GFP, modified poly-GA or modified poly-GR in transduced i^3 Neurons. Neurons were stained using FLAG antibody against the C-terminal FLAG epitope tag in each construct. **(b,c)** Points represent three biological replicates. Data are mean \pm s.e.m.



Extended Data Fig. 5: MeRIP-seq in control and C9ORF72-ALS/FTD iPSNs and postmortem motor cortex.

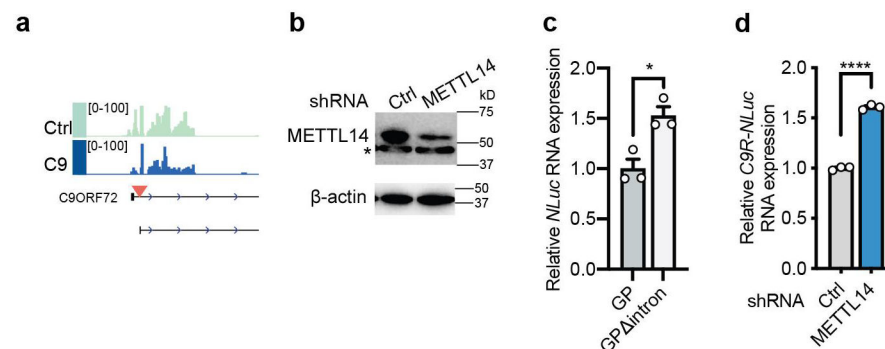
a, Venn diagram depicting the total number and overlaps of m⁶A peaks detected in control and C9ORF72-ALS/FTD groups of iPSN (top) and motor cortex (bottom). **b**, The most enriched consensus m⁶A motifs in all conditions. **c**, Metagene profiles of m⁶A peak density along transcripts with three non-overlapping segments (5' UTR, CDS, and 3' UTR) for control and C9ORF72-ALS/FTD groups. **d**, Principal component analysis (PCA) of control and C9ORF72-ALS/FTD samples. **e**, Gene Ontology (GO) enrichment analysis of hypomethylated genes that were identified in both iPSNs and motor cortex.



Extended Data Fig. 6: The impact of m⁶A hypomethylation on mRNAs.

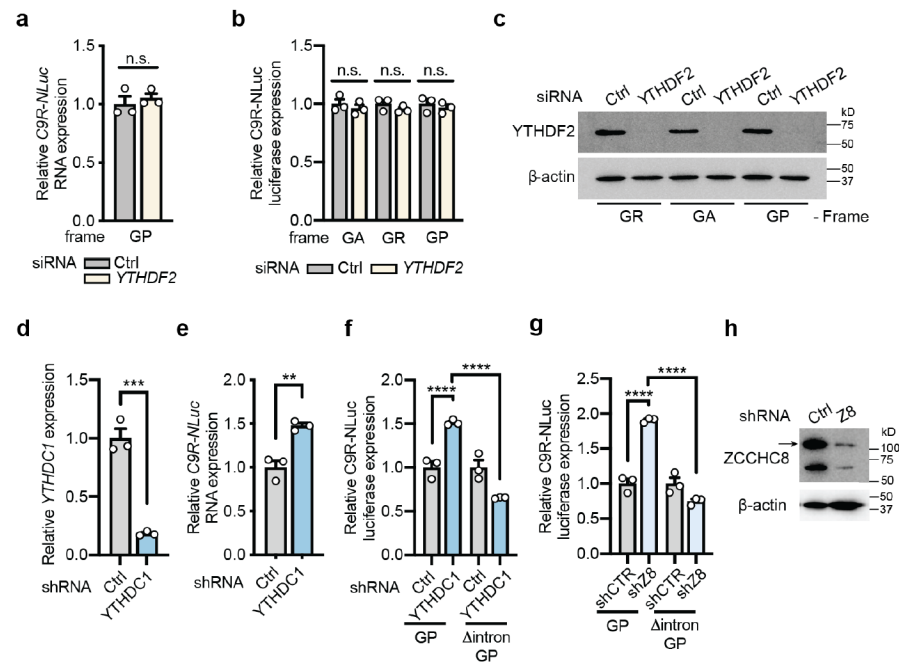
a,b, Volcano plot of differentially expressed genes in C9ORF72-ALS/FTD compared to the control, in iPSNs (**a**) and postmortem motor cortex (**b**). Genes with significant changes are

represented by orange (upregulated in C9) and blue (downregulated in C9) dots. iPSNs: n=4 individual lines per group, 1212 upregulated vs 1168 downregulated. Motor cortex: n=3 individual tissue samples per group, 1892 upregulated versus 1239 downregulated. $p < 0.05$, two-sided. **c**, YTHDF2-RIP qPCR of selected YTHDF2 mRNA targets identified from the non-YTHDF2 bound RNAs. *HPRT1* and *SMARCA1* mRNAs have no m⁶A modification according to the MeRIP-seq results. Points represent individual iPSN lines. n=3 in each group. Data are mean \pm s.e.m. $p = 0.7047$ and $p = 0.4001$, respectively, by two-tailed *t* test. **d**, Cumulative distribution demonstrating the half-life of YTHDF2 targets between control and C9ORF72-ALS/FTD iPSNs. p-value was calculated by a two-tailed non-parametric Wilcoxon-Mann-Whitney test. **e**, Gene Ontology (GO) enrichment analysis of hypomethylated YTHDF2 binding targets which also showed significantly increased half-life.



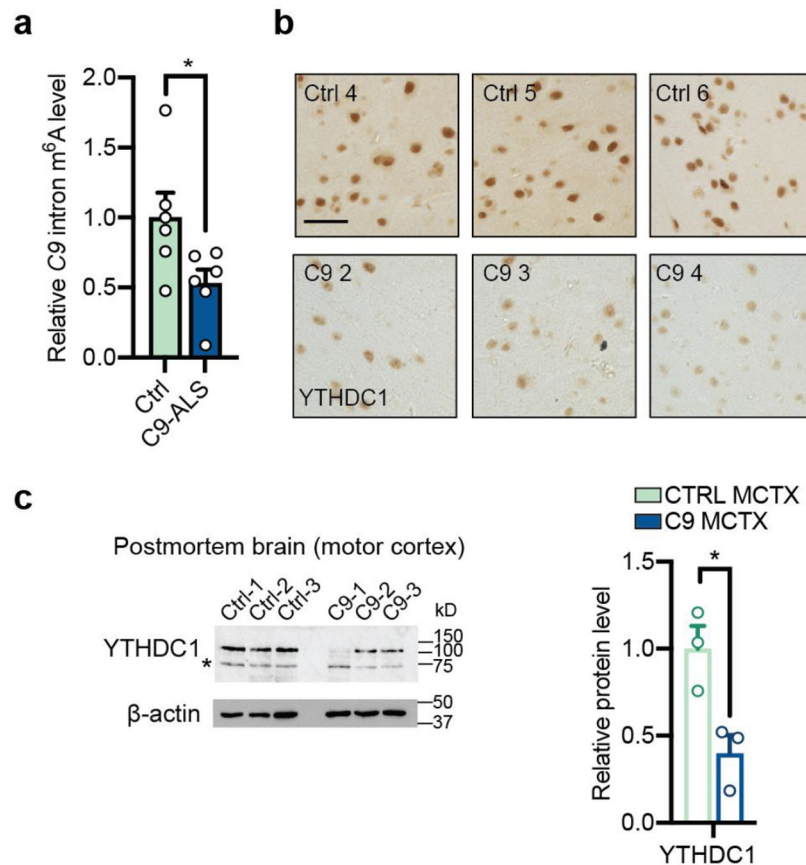
Extended Data Fig. 7: m⁶A regulates C9ORF72 repeat-containing RNA.

a, IGV profile showing the m⁶A peaks (generated by comparing MeRIP against input) in control and C9ORF72-ALS/FTD iPSNs. Red arrow head represents the repeat expansion. **b**, Western blotting of METTL14 in control or METTL14 knockdown i³Neurons. *non-specific band. **c**, The relative basal expression of NLuc RNA in the HeLa Flp-In cells expressing the reporters as described in Fig. 4b. * $p = 0.015$ by two-tailed *t* test. **d**, The relative expression level of C9R-NLuc RNA upon knockdown of METTL14 in i³Neurons, measured by RT-qPCR and normalized to non-targeting shRNA control. **** $p < 0.0001$ by two-tailed *t* test. (c,d) Points represent three biological replicates. Data are mean \pm s.e.m.



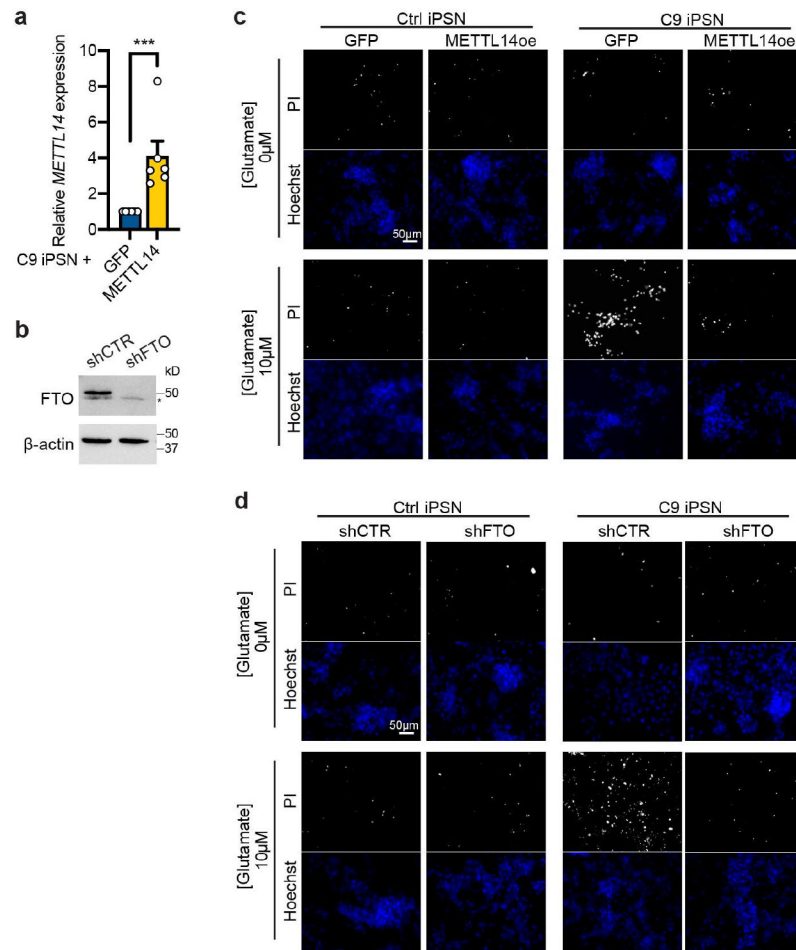
Extended Data Fig. 8: The turnover of *C9ORF72* repeat-containing RNA is regulated by m⁶A in i³Neurons.

a, RT-qPCR of C9 repeat RNA expression from the C9R-NLuc HeLa reporter upon knockdown of YTHDF2. $p=0.5418$ by two-tailed t test. **b**, Relative DPR level was measured by luciferase assay upon YTHDF2 knockdown in the C9R-NLuc HeLa reporter. **c**, Western blotting of YTHDF2 in control or YTHDF2 knockdown HeLa Flp-In cells. $p=0.9456$, 0.8801 and 0.9731 , respectively, by one-way analysis of variance (ANOVA) with Tukey's multiple comparisons. **d,e**, The relative expression level of *YTHDC1* RNA (**d**) or *C9R-NLuc* RNA (**e**) upon knockdown of YTHDC1 by shRNA in i³Neurons. $**p=0.0046$, $***p=0.0006$ by two-tailed t test. **f,g**, Relative DPR levels were measured by luciferase assay upon YTHDC1 knockdown (**f**) or ZCCHC8 knockdown (**g**) in the i³Neurons expressing the reporters in Fig. 4b. NLuc signal was normalized to the total protein level in each sample and the relative expression was compared to non-targeting shRNA control. $****p<0.0001$ by one-way analysis of variance (ANOVA) with Tukey's multiple comparisons. **h**, Western blotting of ZCCHC8 in control or ZCCHC8 knockdown i³Neurons. Arrow points the expected size of ZCCHC8. (**a,b,d-g**) Data are mean \pm s.e.m. Points represent three biological replicates.



Extended Data Fig. 9: m⁶A hypomethylation of the endogenous C9 repeat-containing intron and YTHDC1 expression in the postmortem brain tissues.

a, MeRIP coupled with RT-qPCR of endogenous C9 repeat-containing intronic RNA in control and C9ORF72-ALS/FTD iPSNs. Points represent individual cell lines. $n=6$ per group. $*p=0.0427$. **b**, Representative IHC staining of YTHDC1 at temporal cortex section of control and C9ORF72-ALS/FTD samples. Scale bar = 50 μ m. **c**, Western blotting (left) and quantification (right) of YTHDC1 using postmortem motor cortex tissue samples. $n=3$ individuals per group. *Non-specific bands. $*p=0.0246$. (**a,c**) Data are mean \pm s.e.m. Points represent individual control or patient samples. p -values were calculated by two-tailed t test.



Extended Data Fig. 10: m⁶A restoration reduces glutamate-induced excitotoxicity in C9ORF72-ALS/FTD iPSNs.

a, RT-qPCR of *METTL14* in C9ORF72-ALS/FTD iPSNs expressing exogenous *METTL14* or GFP control. Data are mean \pm s.e.m. Points represent individual cell lines. n=6 in each group. *** $p=0.0006$ by paired two-tailed t test. **b**, Western blotting of FTO in C9ORF72-ALS/FTD iPSNs upon knockdown of FTO by shRNA. *non-specific band. **c,d**, Representative images of Hoechst and propidium iodide (PI) staining of iPSNs in the glutamate-induced excitotoxicity assay. C9ORF72-ALS/FTD iPSNs were infected with lentivirus overexpressing *METTL14* or GFP as negative control (c), or expressing FTO shRNA or non-targeting control shRNA (d).

Supplementary Material

Refer to Web version on PubMed Central for supplementary material.

Acknowledgments

We thank Target ALS Postmortem Tissue Core and Johns Hopkins ALS Postmortem Tissue Core for providing postmortem human brain tissue samples. We thank Dr. Terri Thompson from Answer ALS consortium for providing help and detailed data information. We thank Dr. Michael Ward and his lab at NIH for sharing the i³N iPSC line and the i³Neuron differentiation protocols. We thank Dr. Kevin Talbot at University of Oxford for

providing us the isogenic pair of patient iPSC lines. We thank Lin Xue for the help with the GP ELISA. We thank Dr. Jeffrey Rothstein and his lab for sharing control and patient iPSC lines and protocols. We thank Sun lab members for helpful discussion. This work is supported by Johns Hopkins University Catalyst Award (S.S.), NIH grants R01NS107347 (S.S.), RF1NS113820 (S.S.), R21AG072078 (S.S.), RF1NS127925 (S.S.), HG008935 (C.H.), ES030546 (C.H.), K08NS104273 (L.H.), R01NS123538 (L.H.), and the Packard Center for ALS Research (S.S.). Z.Z. was a recipient of the Milton Safenowitz Post-Doctoral Fellowship from the ALS Association, the Toffler Scholar Award and the Postdoc Development Grant from Muscular Dystrophy Association (MDA). The Mass Spectrometry Facility of the University of Chicago is funded by National Science Foundation (CHE-1048528). C.H. is an investigator of the Howard Hughes Medical Institute.

Data availability

Requests for further information or resources and reagents should be directed to and will be filled by the lead contact, Shuying Sun (shuying.sun@jhmi.edu). Plasmids generated in this study are available from the lead contact upon request. The sequencing data (Supplementary Table 7) have been deposited at the NCBI under GEO accession number GSE203581.

Code availability

This paper does not report original code.

References

1. Nussbacher JK, Tabet R, Yeo GW & Lagier-Tourenne C Disruption of RNA Metabolism in Neurological Diseases and Emerging Therapeutic Interventions. *Neuron* 102, 294–320 (2019). [PubMed: 30998900]
2. Ferrari R, Kapogiannis D, Huey ED & Momeni P FTD and ALS: a tale of two diseases. *Curr Alzheimer Res* 8, 273–94 (2011). [PubMed: 21222600]
3. Ito D, Hatano M & Suzuki N RNA binding proteins and the pathological cascade in ALS/FTD neurodegeneration. *Sci Transl Med* 9(2017).
4. Freibaum BD & Taylor JP The Role of Dipeptide Repeats in C9ORF72-Related ALS-FTD. *Front Mol Neurosci* 10, 35 (2017). [PubMed: 28243191]
5. Cheng W. et al. CRISPR-Cas9 Screens Identify the RNA Helicase DDX3X as a Repressor of C9ORF72 (GGGGCC)_n Repeat-Associated Non-AUG Translation. *Neuron* 104, 885–898.e8 (2019). [PubMed: 31587919]
6. Dominissini D. et al. Topology of the human and mouse m⁶A RNA methylomes revealed by m⁶A-seq. *Nature* 485, 201–6 (2012). [PubMed: 22575960]
7. Meyer KD et al. Comprehensive analysis of mRNA methylation reveals enrichment in 3' UTRs and near stop codons. *Cell* 149, 1635–46 (2012). [PubMed: 22608085]
8. Liu J. et al. A METTL3-METTL14 complex mediates mammalian nuclear RNA N⁶-adenosine methylation. *Nat Chem Biol* 10, 93–5 (2014). [PubMed: 24316715]
9. Roundtree IA, Evans ME, Pan T & He C Dynamic RNA Modifications in Gene Expression Regulation. *Cell* 169, 1187–1200 (2017). [PubMed: 28622506]
10. Jia G. et al. N⁶-methyladenosine in nuclear RNA is a major substrate of the obesity-associated FTO. *Nat Chem Biol* 7, 885–7 (2011). [PubMed: 22002720]
11. Zheng G. et al. ALKBH5 is a mammalian RNA demethylase that impacts RNA metabolism and mouse fertility. *Mol Cell* 49, 18–29 (2013). [PubMed: 23177736]
12. Xiao W. et al. Nuclear m⁶A Reader YTHDC1 Regulates mRNA Splicing. *Mol Cell* 61, 507–519 (2016). [PubMed: 26876937]
13. Du H. et al. YTHDF2 destabilizes m⁶A-containing RNA through direct recruitment of the CCR4-NOT deadenylase complex. *Nat Commun* 7, 12626 (2016). [PubMed: 27558897]
14. Wang X. et al. N⁶-methyladenosine Modulates Messenger RNA Translation Efficiency. *Cell* 161, 1388–99 (2015). [PubMed: 26046440]

15. Wang X. et al. N6-methyladenosine-dependent regulation of messenger RNA stability. *Nature* 505, 117–20 (2014). [PubMed: 24284625]
16. Liu J. et al. Landscape and Regulation of m⁶A and m⁶Am Methylome across Human and Mouse Tissues. *Mol Cell* 77, 426–440.e6 (2020). [PubMed: 31676230]
17. Livneh I, Moshitch-Moshkovitz S, Amariglio N, Rechavi G & Dominissini D The m⁶A epitranscriptome: transcriptome plasticity in brain development and function. *Nat Rev Neurosci* 21, 36–51 (2020). [PubMed: 31804615]
18. Deng X. et al. Widespread occurrence of N6-methyladenosine in bacterial mRNA. *Nucleic Acids Res* 43, 6557–67 (2015). [PubMed: 26068471]
19. Tian R. et al. CRISPR Interference-Based Platform for Multimodal Genetic Screens in Human iPSC-Derived Neurons. *Neuron* 104, 239–255.e12 (2019). [PubMed: 31422865]
20. Mackenzie IR et al. Quantitative analysis and clinico-pathological correlations of different dipeptide repeat protein pathologies in C9ORF72 mutation carriers. *Acta Neuropathol* 130, 845–61 (2015). [PubMed: 26374446]
21. Mori K. et al. The C9orf72 GGGGCC repeat is translated into aggregating dipeptide-repeat proteins in FTL/ALS. *Science* 339, 1335–8 (2013). [PubMed: 23393093]
22. Cheng W. et al. C9ORF72 GGGGCC repeat-associated non-AUG translation is upregulated by stress through eIF2 α phosphorylation. *Nat Commun* 9, 51 (2018). [PubMed: 29302060]
23. Wang S. et al. Nuclear export and translation of circular repeat-containing intronic RNA in C9ORF72-ALS/FTD. *Nat Commun* 12, 4908 (2021). [PubMed: 34389711]
24. Liu J. et al. N⁶-methyladenosine of chromosome-associated regulatory RNA regulates chromatin state and transcription. *Science* 367, 580–586 (2020). [PubMed: 31949099]
25. Lubas M. et al. Interaction profiling identifies the human nuclear exosome targeting complex. *Mol Cell* 43, 624–37 (2011). [PubMed: 21855801]
26. Mori K. et al. Bidirectional transcripts of the expanded C9orf72 hexanucleotide repeat are translated into aggregating dipeptide repeat proteins. *Acta Neuropathol* 126, 881–93 (2013). [PubMed: 24132570]
27. Lagier-Tourenne C. et al. Targeted degradation of sense and antisense C9orf72 RNA foci as therapy for ALS and frontotemporal degeneration. *Proc Natl Acad Sci U S A* 110, E4530–9 (2013). [PubMed: 24170860]
28. Gendron TF et al. Antisense transcripts of the expanded C9ORF72 hexanucleotide repeat form nuclear RNA foci and undergo repeat-associated non-ATG translation in c9FTD/ALS. *Acta Neuropathol* 126, 829–44 (2013). [PubMed: 24129584]
29. Mizielinska S. et al. C9orf72 frontotemporal lobar degeneration is characterised by frequent neuronal sense and antisense RNA foci. *Acta Neuropathol* 126, 845–57 (2013). [PubMed: 24170096]
30. Zu T. et al. RAN proteins and RNA foci from antisense transcripts in C9ORF72 ALS and frontotemporal dementia. *Proc Natl Acad Sci U S A* 110, E4968–77 (2013). [PubMed: 24248382]
31. Jiang J. et al. Gain of Toxicity from ALS/FTD-Linked Repeat Expansions in C9ORF72 Is Alleviated by Antisense Oligonucleotides Targeting GGGGCC-Containing RNAs. *Neuron* 90, 535–50 (2016). [PubMed: 27112497]
32. Donnelly CJ et al. RNA toxicity from the ALS/FTD C9ORF72 expansion is mitigated by antisense intervention. *Neuron* 80, 415–28 (2013). [PubMed: 24139042]
33. Huang Y. et al. Small-Molecule Targeting of Oncogenic FTO Demethylase in Acute Myeloid Leukemia. *Cancer Cell* 35, 677–691.e10 (2019). [PubMed: 30991027]
34. Su R. et al. Targeting FTO Suppresses Cancer Stem Cell Maintenance and Immune Evasion. *Cancer Cell* 38, 79–96 e11 (2020). [PubMed: 32531268]
35. Liu Y. et al. Tumors exploit FTO-mediated regulation of glycolytic metabolism to evade immune surveillance. *Cell Metab* 33, 1221–1233 e11 (2021). [PubMed: 33910046]
36. Jiang X. et al. The role of m⁶A modification in the biological functions and diseases. *Signal Transduct Target Ther* 6, 74 (2021). [PubMed: 33611339]
37. Lence T. et al. m⁶A modulates neuronal functions and sex determination in *Drosophila*. *Nature* 540, 242–247 (2016). [PubMed: 27919077]

38. Wang CX et al. METTL3-mediated m⁶A modification is required for cerebellar development. *PLoS Biol* 16, e2004880 (2018). [PubMed: 29879109]
39. Devlin AC et al. Human iPSC-derived motoneurons harbouring TARDBP or C9ORF72 ALS mutations are dysfunctional despite maintaining viability. *Nat Commun* 6, 5999 (2015). [PubMed: 25580746]
40. Wainger BJ et al. Intrinsic membrane hyperexcitability of amyotrophic lateral sclerosis patient-derived motor neurons. *Cell Rep* 7, 1–11 (2014). [PubMed: 24703839]
41. Koranda JL et al. Mettl14 Is Essential for Epitranscriptomic Regulation of Striatal Function and Learning. *Neuron* 99, 283–292 e5 (2018). [PubMed: 30056831]
42. Lall D. et al. C9orf72 deficiency promotes microglial-mediated synaptic loss in aging and amyloid accumulation. *Neuron* 109, 2275–2291.e8 (2021). [PubMed: 34133945]
43. Zhu Q. et al. Reduced C9ORF72 function exacerbates gain of toxicity from ALS/FTD-causing repeat expansion in C9orf72. *Nat Neurosci* 23, 615–624 (2020). [PubMed: 32284607]
44. Schmitz A, Pinheiro Marques J, Oertig I, Maharjan N & Saxena S Emerging Perspectives on Dipeptide Repeat Proteins in C9ORF72 ALS/FTD. *Front Cell Neurosci* 15, 637548 (2021). [PubMed: 33679328]
45. McEachin ZT, Parameswaran J, Raj N, Bassell GJ & Jiang J RNA-mediated toxicity in C9orf72 ALS and FTD. *Neurobiol Dis* 145, 105055 (2020). [PubMed: 32829028]
46. Donnelly CJ, Grima JC & Sattler R Aberrant RNA homeostasis in amyotrophic lateral sclerosis: potential for new therapeutic targets? *Neurodegener Dis Manag* 4, 417–37 (2014). [PubMed: 25531686]
47. Conlon EG et al. The C9ORF72 GGGGCC expansion forms RNA G-quadruplex inclusions and sequesters hnRNP H to disrupt splicing in ALS brains. *Elife* 5(2016).
48. Lee YB et al. Hexanucleotide repeats in ALS/FTD form length-dependent RNA foci, sequester RNA binding proteins, and are neurotoxic. *Cell Rep* 5, 1178–86 (2013). [PubMed: 24290757]
49. Sareen D. et al. Targeting RNA foci in iPSC-derived motor neurons from ALS patients with a C9ORF72 repeat expansion. *Sci Transl Med* 5, 208ra149 (2013).
50. Xu Z. et al. Expanded GGGGCC repeat RNA associated with amyotrophic lateral sclerosis and frontotemporal dementia causes neurodegeneration. *Proc Natl Acad Sci U S A* 110, 7778–83 (2013). [PubMed: 23553836]
51. McMillan M. et al. RNA methylation influences TDP43 binding and disease pathogenesis in models of amyotrophic lateral sclerosis and frontotemporal dementia. *Molecular Cell* (2023).
52. Zhao F. et al. METTL3-dependent RNA m⁶A dysregulation contributes to neurodegeneration in Alzheimer's disease through aberrant cell cycle events. *Mol Neurodegener* 16, 70 (2021). [PubMed: 34593014]
53. Association, A.s. 2016 Alzheimer's disease facts and figures. *Alzheimers Dement* 12, 459–509 (2016). [PubMed: 27570871]
54. Shafik AM et al. N6-methyladenosine dynamics in neurodevelopment and aging, and its potential role in Alzheimer's disease. *Genome Biol* 22, 17 (2021). [PubMed: 33402207]
55. Chen X. et al. Down-Regulation of m⁶A mRNA Methylation Is Involved in Dopaminergic Neuronal Death. *ACS Chem Neurosci* 10, 2355–2363 (2019). [PubMed: 30835997]
56. Cleary EM et al. Improved PCR based methods for detecting C9orf72 hexanucleotide repeat expansions. *Mol Cell Probes* 30, 218–224 (2016). [PubMed: 27288208]

Methods-only references

57. Zaepfel BL et al. UPF1 reduces C9orf72 HRE-induced neurotoxicity in the absence of nonsense-mediated decay dysfunction. *Cell Rep* 34, 108925 (2021). [PubMed: 33789100]
58. Coyne AN et al. Nuclear accumulation of CHMP7 initiates nuclear pore complex injury and subsequent TDP-43 dysfunction in sporadic and familial ALS. *Sci Transl Med* 13(2021).
59. Bolger AM, Lohse M & Usadel B Trimmomatic: a flexible trimmer for Illumina sequence data. *Bioinformatics* 30, 2114–20 (2014). [PubMed: 24695404]

60. Kim D, Paggi JM, Park C, Bennett C & Salzberg SL Graph-based genome alignment and genotyping with HISAT2 and HISAT-genotype. *Nat Biotechnol* 37, 907–915 (2019). [PubMed: 31375807]
61. Danecek P. et al. Twelve years of SAMtools and BCFtools. *Gigascience* 10(2021).
62. Zhang Y. et al. Model-based analysis of ChIP-Seq (MACS). *Genome Biol* 9, R137 (2008). [PubMed: 18798982]
63. Cui X. et al. MeTDiff: A Novel Differential RNA Methylation Analysis for MeRIP-Seq Data. *IEEE/ACM Trans Comput Biol Bioinform* 15, 526–534 (2018). [PubMed: 29610101]
64. Anders S, Pyl PT & Huber W HTSeq--a Python framework to work with high-throughput sequencing data. *Bioinformatics* 31, 166–9 (2015). [PubMed: 25260700]
65. Love MI, Huber W & Anders S Moderated estimation of fold change and dispersion for RNA-seq data with DESeq2. *Genome Biol* 15, 550 (2014). [PubMed: 25516281]
66. Robinson MD, McCarthy DJ & Smyth GK edgeR: a Bioconductor package for differential expression analysis of digital gene expression data. *Bioinformatics* 26, 139–40 (2010). [PubMed: 19910308]
67. Heinz S. et al. Simple combinations of lineage-determining transcription factors prime cis-regulatory elements required for macrophage and B cell identities. *Mol Cell* 38, 576–89 (2010). [PubMed: 20513432]
68. Dennis G. et al. DAVID: Database for Annotation, Visualization, and Integrated Discovery. *Genome Biol* 4, P3 (2003). [PubMed: 12734009]
69. Sherman BT et al. DAVID: a web server for functional enrichment analysis and functional annotation of gene lists (2021 update). *Nucleic Acids Res* (2022).
70. Huang DW et al. DAVID Bioinformatics Resources: expanded annotation database and novel algorithms to better extract biology from large gene lists. *Nucleic Acids Res* 35, W169–75 (2007). [PubMed: 17576678]
71. Ababneh NA et al. Correction of amyotrophic lateral sclerosis related phenotypes in induced pluripotent stem cell-derived motor neurons carrying a hexanucleotide expansion mutation in C9orf72 by CRISPR/Cas9 genome editing using homology-directed repair. *Hum Mol Genet* 29, 2200–2217 (2020). [PubMed: 32504093]

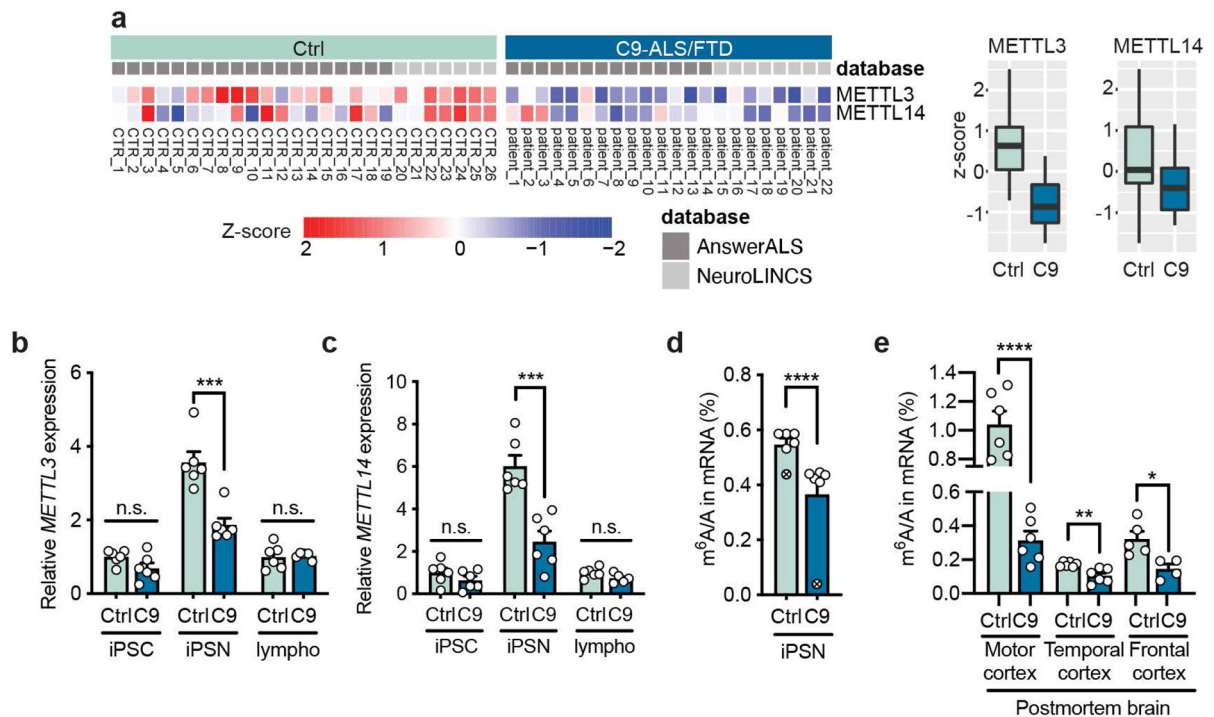


Fig. 1: The expression of *m*⁶A methyltransferases and the *m*⁶A RNA modification levels are downregulated in C9ORF72-ALS/FTD.

a, Proteomic heatmap (left) and boxplots (right) of the *m*⁶A “writer” complex core components in the iPSNs of control (n=26) and C9ORF72-ALS/FTD patients (n=22). Data were analyzed using the proteomic database from Answer ALS and NeuroLINCS center. Batch controls were used for normalization of the AnswerALS data. Box plots indicate the interquartile range with the central line representing the median, and the vertical lines extend to the extreme values in the group. **b,c**, *METTL3* (**b**) and (**c**) *METTL14* RNA expression levels were measured by RT-qPCR in control and C9 iPSC, iPSN and lymphoblast cells. Points represent individual cell lines, including one pair with isogenic control in which the repeat expansion was removed⁷¹. The isogenic control iPSC was set to 1. n=6 for both control and patient iPSC lines. n=6 for control and 5 for C9ORF72-ALS lymphoblast lines. Data are mean ± s.e.m. *METTL3*: iPSC, *p*=0.1042; iPSN, *****p*=0.0006; lympho, *p*=0.8356. *METTL14*: iPSC, *p*=0.2328; iPSN, *****p*=0.0006; lympho, *p*=0.0944. Two-tailed *t* test. **d**, UHPLC-QQQ-MS/MS quantification of the *m*⁶A/A ratio in mRNAs from iPSNs. The mRNAs of the isogenic pair (circle-cross) were extracted by poly-A selection; the mRNAs of the other iPSN lines were extracted by ribosomal RNA depletion. Two-tailed *t* test was performed on 5 pairs of control and C9 lines (ribosomal RNA depletion samples). Data are mean ± s.e.m. *****p*<0.0001 by two-tailed *t* test. **e**, UHPLC-QQQ-MS/MS quantification of the *m*⁶A/A ratio in mRNAs from postmortem brain tissues extracted by poly-A selection. Points represent individual patient samples. n=6 for both control and patient samples. Data are mean ± s.e.m. **p*=0.0168, ***p*=0.0039, *****p*<0.0001, by two-tailed *t* test.

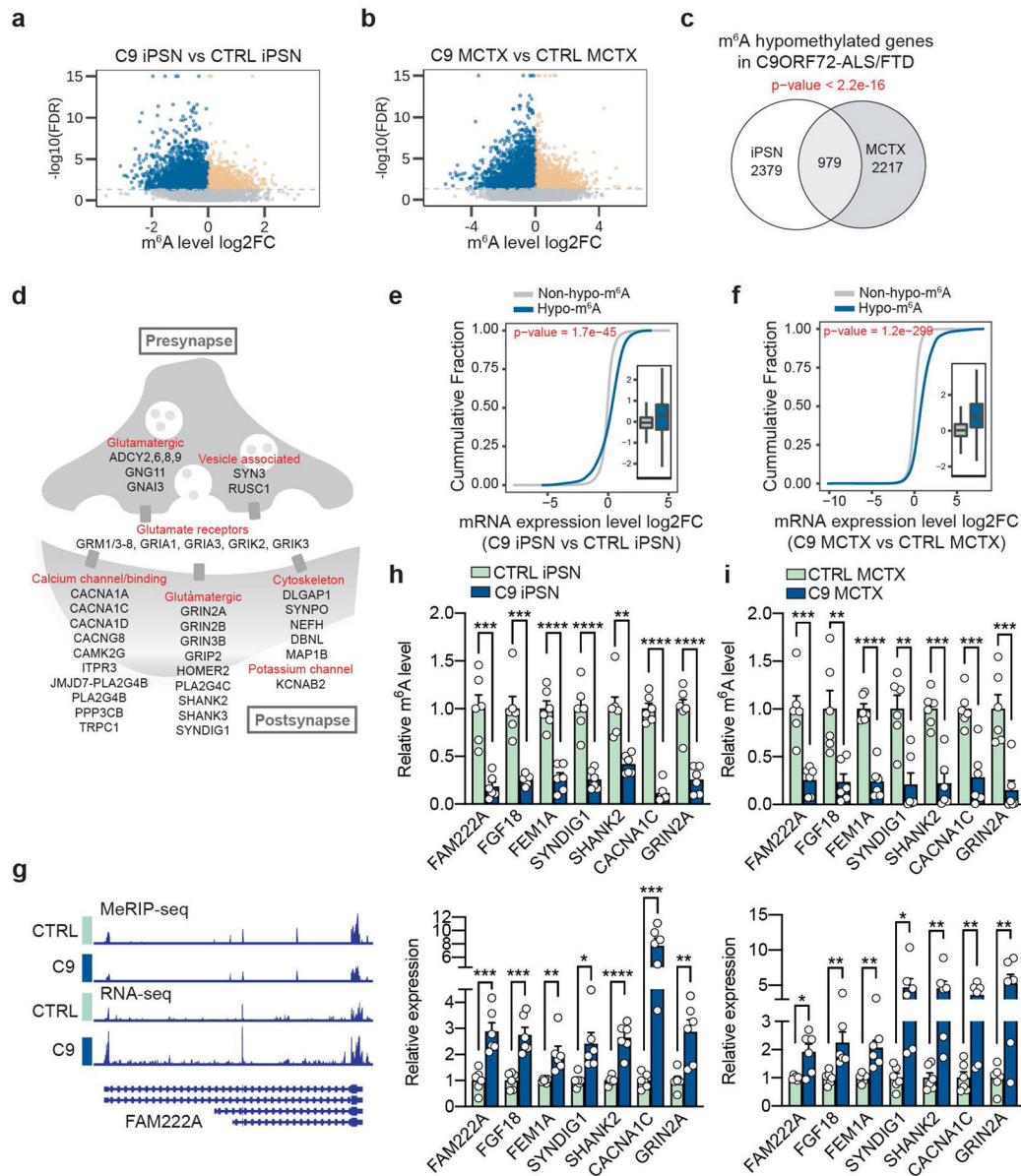


Fig. 2: m⁶A hypomethylation dysregulates neuronal gene expression in C9ORF72-ALS/FTD. **a,b,** Volcano plot of genes with differential m⁶A level between control and C9ORF72-ALS/FTD in iPSNs (**a**) and in human postmortem motor cortex (**b**). iPSN: *n*=4 individual lines per group, 4037 hypomethylated (blue) vs 1494 hypermethylated (orange); Motor cortex (MCTX): *n*=3 individual tissue samples per group, 4146 hypomethylated vs 2091 hypermethylated. FDR < 0.01. **c,** Venn diagram depicting the overlaps of hypomethylated genes between iPSN and motor cortex. p-value was calculated by two-tailed Fisher's exact test. **d,** Schematic of hypomethylated genes related to synaptic functions shared between iPSN and MCTX. **e,f,** Cumulative distribution and boxplot (inside) of mRNA expression changes with or without hypo-m⁶A in patient iPSNs (**e**) and motor cortex (**f**). iPSN: *n*=4 individual lines per group; MCTX: *n*=3 individual tissue samples per group. p-values were calculated by a two-tailed non-parametric Wilcoxon-Matt-Whitney test. Box plots indicate

the interquartile range with the central line representing the median, and the vertical lines extend to the extreme values in the group. **g**, IGV profiles showing m⁶A signal (generated by comparing MeRIP against input) and RNA-seq reads in the selected mRNA target, *FAM222A*. **h,i**, The m⁶A level measured by MeRIP-RT-qPCR (Top) and the relative RNA expression quantified by RT-qPCR (Bottom) of selected transcripts in iPSNs (**h**) and motor cortex (**i**). Points represent individual control or patient iPSN lines ($n=6$ per group) or tissue samples ($n=6$ per group). The isogenic control was set to 1. Data are mean \pm s.e.m. * $p<0.05$, ** $p<0.01$, *** $p<0.001$, **** $p<0.0001$, by paired two-tailed t test.

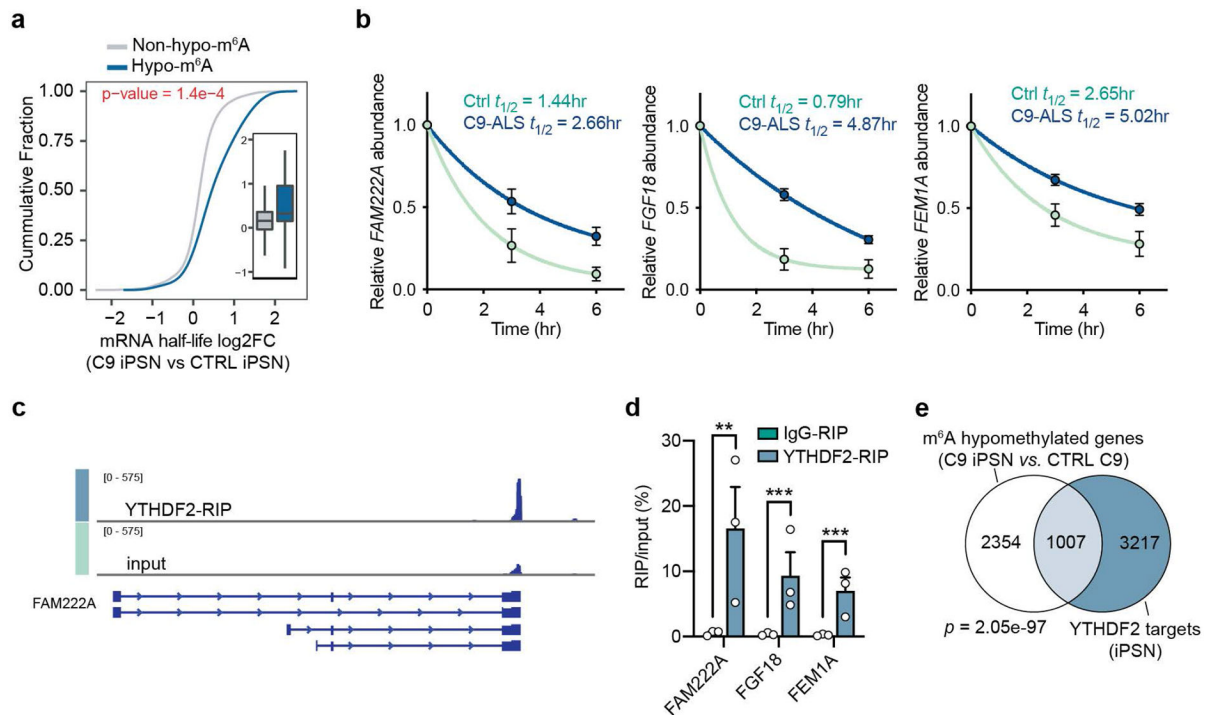


Fig. 3: m⁶A hypomethylation increases mRNA half-life via YTHDF2 in iPSNs.

a, Cumulative distribution and boxplot (inside) of mRNA half-life changes in control and C9ORF72-ALS/FTD iPSNs. $n=3$ individual lines per group. p-value was calculated by a two-tailed non-parametric Wilcoxon-Matt-Whitney test. Box plots indicate the median, first and third quartiles and range. **b**, Half-life of the representative mRNA targets in control and C9ORF72-ALS/FTD iPSNs. The RNA level was measured by RT-qPCR at each time point and normalized to the data at time 0. $n=3$ individual control or C9ORF72-ALS/FTD iPSN lines. Data are mean \pm s.e.m. **c**, IGV profiles showing YTHDF2 binding signal in the selected mRNA target, *FAM222A*. **d**, YTHDF2-RIP qPCR of selected YTHDF2 mRNA targets identified from the YTHDF2-RIP-seq. $n=5$ control iPSN lines. Points represent individual cell lines. Data are mean \pm s.e.m. *FAM222A*, ** $p=0.003$; *FGF18*, *** $p=0.0001$; *FEM1A*, *** $p=0.0006$; by two-tailed t test. **e**, Venn diagram depicting the overlaps of hypomethylated genes and YTHDF2 targets. p-value was calculated by two-tailed Fisher's exact test.

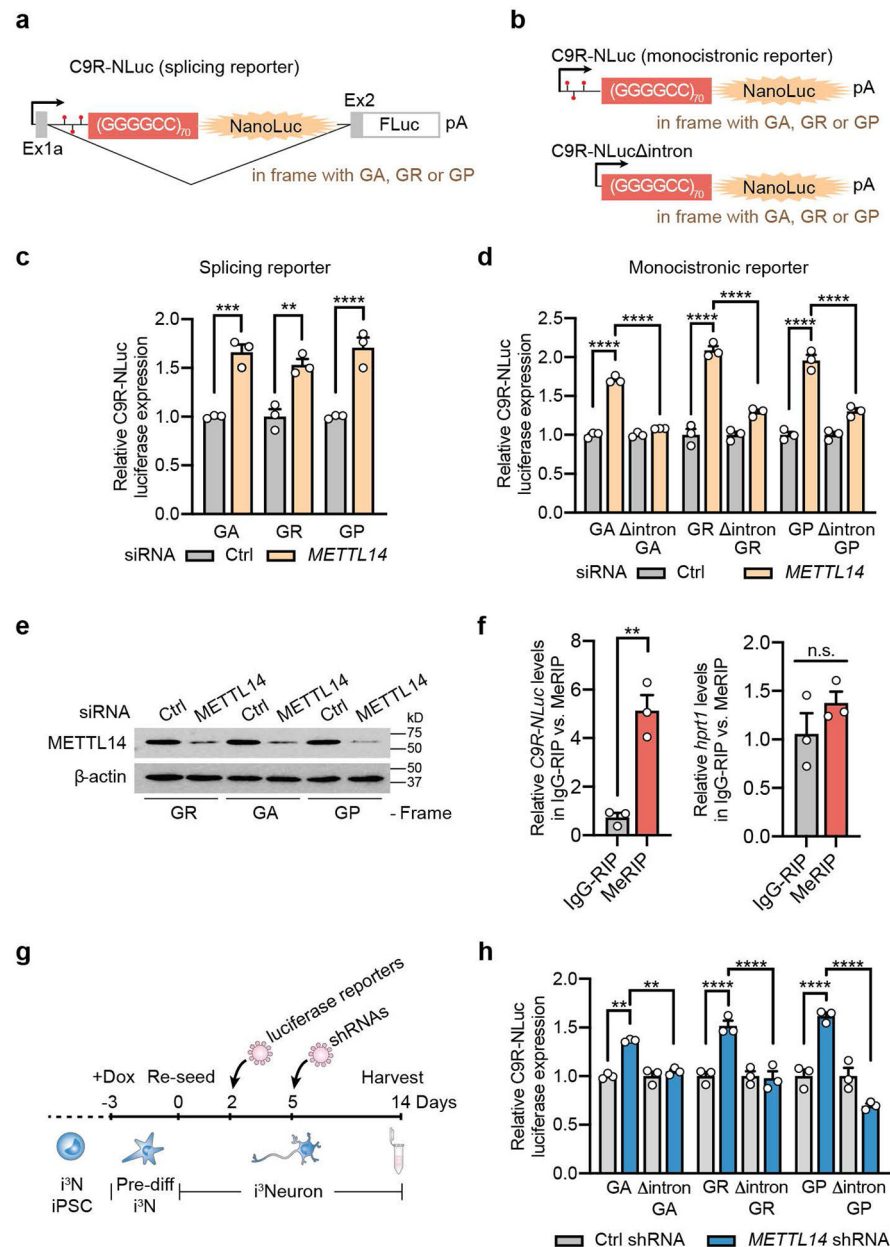


Fig. 4: The m⁶A modification in the repeat-containing intron modulates DPR protein production.

a, Schematic of the bicistronic splicing reporter for (GGGGCC)₇₀ RAN translation, which mimics the splicing of C9 repeat RNA from the endogenous context. Predicted m⁶A sites were indicated as red lollipops in the intron sequence upstream of the repeats. **b**, Schematic of the monocistronic mRNA luciferase reporters for (GGGGCC)₇₀ RAN translation with or without the intronic sequence. Predicted m⁶A sites were indicated as red lollipops. **c**, Relative DPR levels were measured by luciferase assay upon METTL14 knockdown in the HeLa Flp-In cells expressing the reporters in (a). NLuc signal was normalized to the total protein level in each sample and the relative expression was compared to non-targeting siRNA control. Data are mean ± s.e.m. GA, ****p*=0.0002; GR, ***p*=0.0013; GP, *****p*<0.0001, by one-way analysis of variance (ANOVA) with Tukey's multiple

comparisons. **d**, Relative DPR levels were measured by luciferase assay upon METTL14 knockdown in the HeLa Flp-In cells expressing the reporters in **(b)**. NLuc signal was normalized to the total protein level in each sample and the relative expression was compared to non-targeting siRNA control. Data are mean \pm s.e.m. **** $p < 0.0001$, by one-way analysis of variance (ANOVA) with Tukey's multiple comparisons. **e**, Western blotting of METTL14 in non-targeting or METTL14 siRNA transfected HeLa Flp-In cells. β -actin was blotted as internal control. **f**, RNA immunoprecipitation by IgG or m⁶A antibody (MeRIP) followed by RT-qPCR of *HPRT1* RNA (left) or *C9* repeat RNA (right) in the HeLa Flp-In C9R-NLuc reporter cells. *HPRT1* RNA does not have m⁶A modification and serves as a negative control. Data are mean \pm s.e.m. Points represent three biological replicates. *C9R-NLuc*, ** $p = 0.0028$; *HPRT1*, $p = 0.2584$, by two-tailed *t* test. **g**, Timeline for the luciferase reporter experiments in human i³Neurons. **h**, Relative DPR levels were measured by luciferase assay upon METTL14 knockdown in the i³Neurons expressing the reporters as described in **(g)**. $n = 3$ biological replicates. Data are mean \pm s.e.m. ** $p = 0.001$ and 0.0053 , respectively, **** $p < 0.0001$, by one-way analysis of variance (ANOVA) with Tukey's multiple comparisons. Points represent three biological replicates in each group.

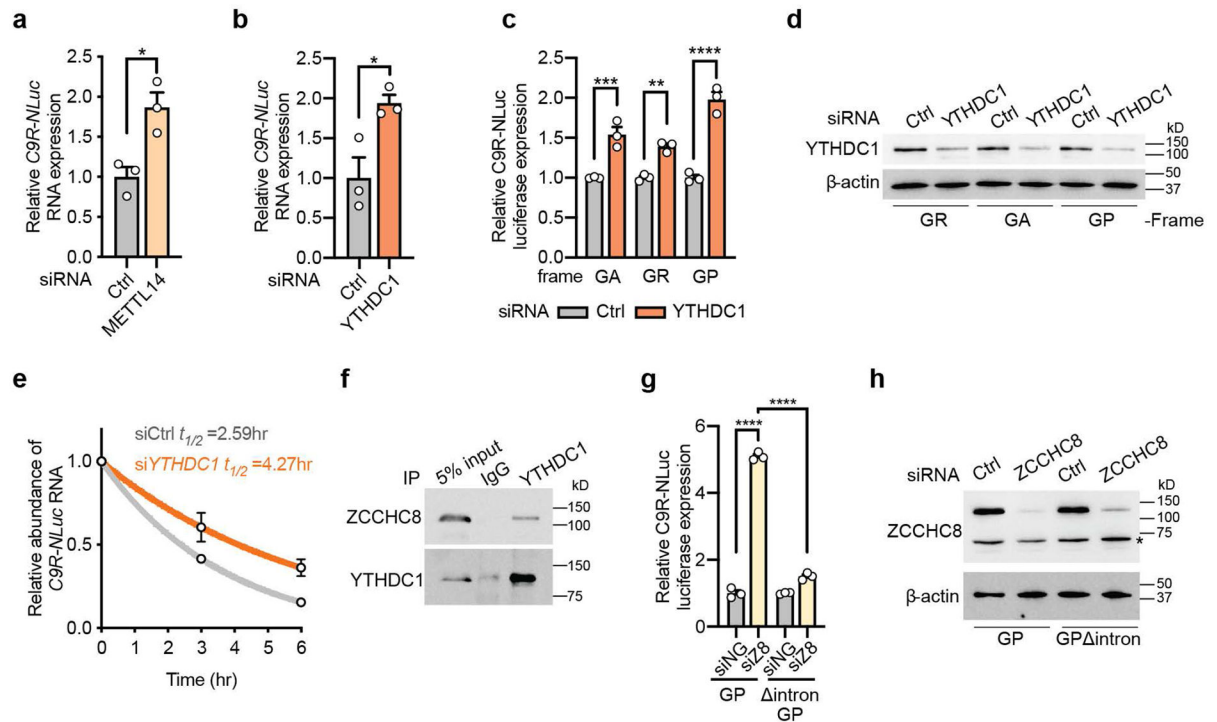


Fig. 5: YTHDC1 regulates the stability of *C9ORF72* repeat-containing intron RNA via the NEXT decay pathway.

a,b, The relative expression level of *C9R-NLuc* RNA upon knockdown of METTL14 (**a**) or YTHDC1 (**b**) measured by RT-qPCR and normalized to non-targeting siRNA control. * $p=0.0175$ (**a**), * $p=0.0283$ (**b**) by two-tailed t test. **c,** Relative DPR levels were measured by luciferase assay upon YTHDC1 knockdown. NLuc signals were normalized to the total protein level. ** $p=0.0062$, *** $p=0.0004$, **** $p<0.0001$ by one-way analysis of variance (ANOVA) with Tukey's multiple comparisons. **d,** Western blotting of YTHDC1 in non-targeting or YTHDC1 siRNA transfected HeLa Flp-In cells. **e,** Half-life of *C9* repeat RNA in HeLa *C9R-NLuc* reporter cells transfected with YTHDC1 siRNA or non-targeting control. The RNA level was measured by RT-qPCR at each time point and normalized to the data at time 0. **f,** Immunoprecipitation was performed in human iPSNs with YTHDC1 antibody or IgG control. The input and precipitated proteins were immunoblotted with YTHDC1 and ZCCHC8 antibodies. $n = 3$ biological replicates. **g,** Relative DPR levels were measured by luciferase assay upon ZCCHC8 knockdown. **** $p<0.0001$ by one-way analysis of variance (ANOVA) with Tukey's multiple comparisons. **h,** Western blotting of ZCCHC8 in control or ZCCHC8 knockdown HeLa Flp-In cells. *non-specific band. (**a-c,e,g**) Data are mean \pm s.e.m. Points represent three biological replicates at each condition.

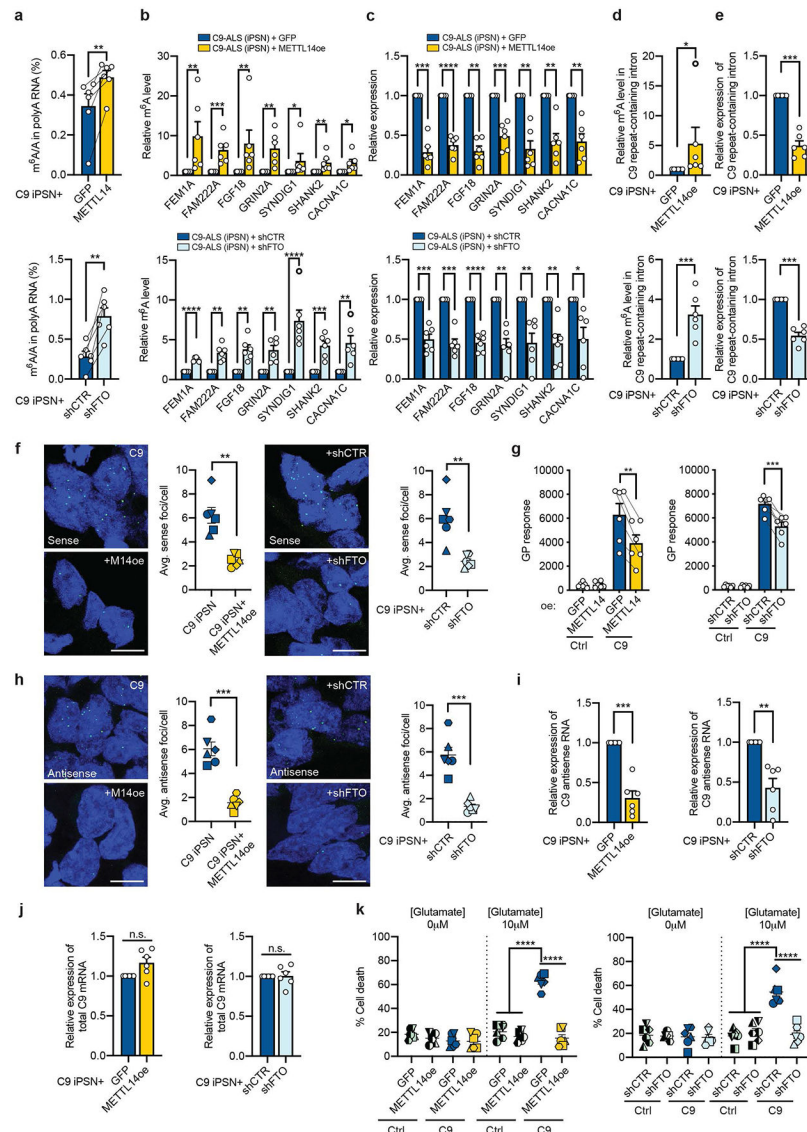


Fig. 6: m⁶A restoration rescues disease-related phenotypes in C9ORF72-ALS/FTD patient iPSNs.

C9ORF72-ALS/FTD iPSNs were infected with lentivirus overexpressing METTL14 or GFP as negative control, or with lentivirus expressing FTO shRNA or non-targeting control shRNA. Data are from six patient iPSN lines. Points represent individual lines. **a**, UHPLC-QQQ-MS/MS quantification of the m⁶A/A ratio in poly-A RNAs from iPSNs with METTL14 overexpression (Top) or FTO knockdown (Bottom). ***p*=0.0043 and 0.0012, respectively, by paired two-tailed *t* test. **b**, The m⁶A level of representative mRNA targets was examined by MeRIP coupled with RT-qPCR. (Top) Overexpression of METTL14. (Bottom) Knockdown of FTO. **p*<0.05, ***p*<0.01, ****p*<0.001, *****p*<0.0001, by paired two-tailed *t* test. **c**, The RNA expression of the targets was examined by RT-qPCR. (Top) Overexpression of METTL14. (Bottom) Knockdown of FTO. **p*<0.05, ***p*<0.01, ****p*<0.001, *****p*<0.0001, by paired two-tailed *t* test. **d**, Relative m⁶A level in the C9 repeat-containing intron was measured by MeRIP-RT-qPCR. **p*=0.0319, ****p*=0.0005, by

paired two-tailed *t* test. **e**, Relative RNA expression of *C9* repeat-containing intron was measured by RT-qPCR. ****p*=0.0001 by paired two-tailed *t* test. **f,h**, Representative images and quantification of FISH experiment to examine the sense (**f**) and antisense (**h**) RNA foci changes in C9ORF72-ALS/FTD iPSNs upon METTL14 overexpression (Left) or FTO knockdown (Right). Scale bar, 10μm. ***p*=0.0044 and 0.0058, respectively (f); ****p*=0.0001 and 0.0009, respectively (h), by paired two-tailed *t* test. **g**, Poly-GP protein level was measured by ELISA. (Left) Overexpression of METTL14. (Right) Knockdown of FTO. ***p*=0.0024, ****p*=0.001, by paired two-tailed *t* test. **i**, RT-qPCR of endogenous antisense repeat RNA expression in C9ORF72-ALS/FTD iPSNs upon METTL14 overexpression (Left) or FTO knockdown (Right). ***p*=0.0046, ****p*=0.0005, by paired two-tailed *t* test. **j**, RT-qPCR of total C9 mRNA expression in C9ORF72-ALS/FTD iPSNs upon METTL14 overexpression (Left) or FTO knockdown (Right). *p*=0.0617 and 0.9238, respectively. **k**, Glutamate-induced excitotoxicity in control and C9ORF72-ALS/FTD iPSNs overexpressing GFP vs METTL14, or expressing control shRNA vs FTO shRNA. Different shapes represent different iPSN lines from 6 control and 6 patients. *****p*<0.0001 by paired two-tailed *t* test. (**a-k**) Data are mean ± s.e.m. Points represent individual cell lines.

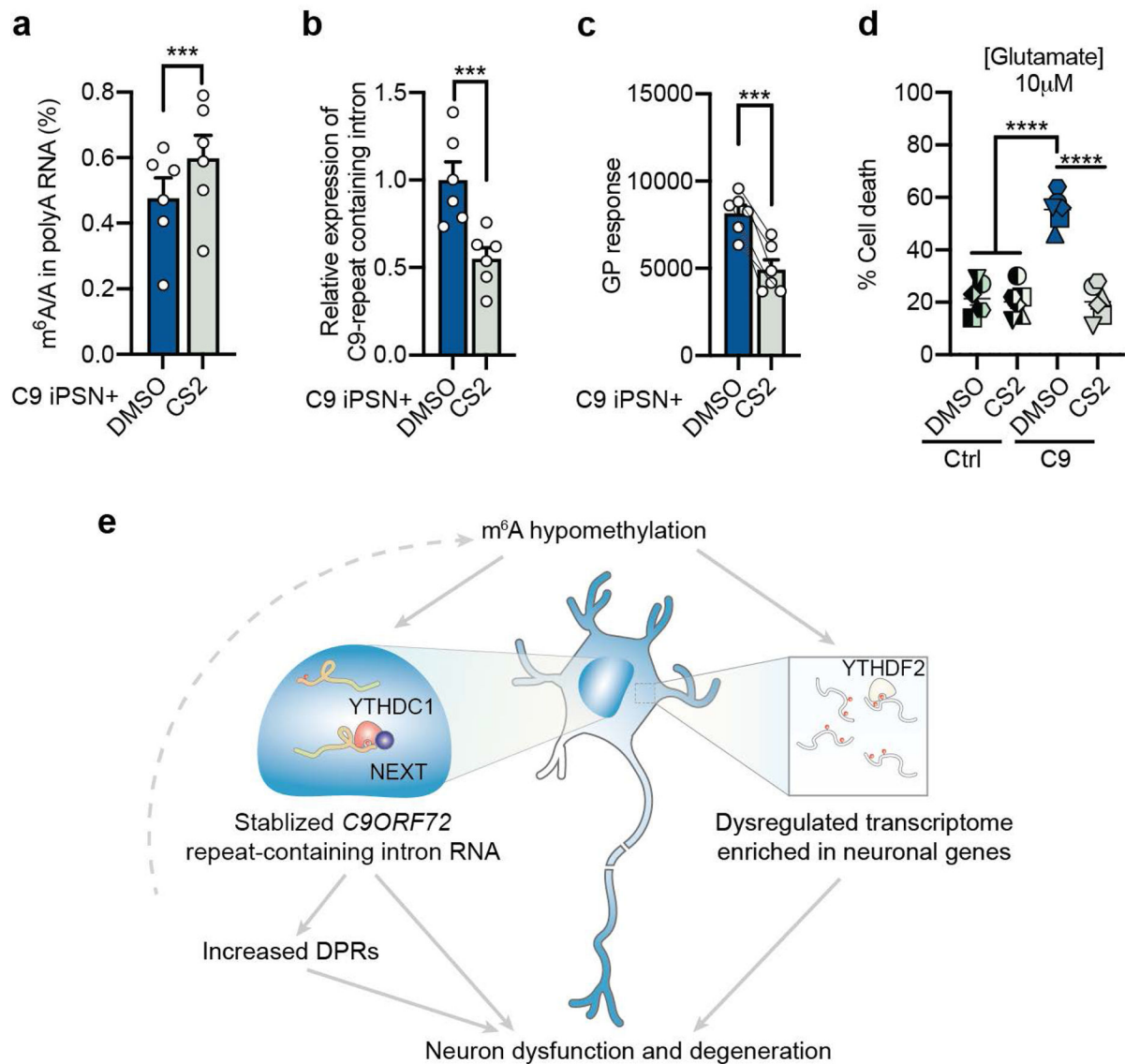


Fig. 7: FTO inhibitor treatment mitigates disease phenotypes.

a, UHPLC-QQQ-MS/MS quantification of the m⁶A/A ratio in poly-A RNAs from iPSNs with CS2 (500nM) treatment for 7 days. *** $p=0.0003$ by paired two-tailed t test. **b,c**, Relative expression of *C9* repeat-containing intron RNA (**b**) and poly-GP protein level (**c**) in *C9ORF72*-ALS/FTD iPSNs after treatment with DMSO control or FTO inhibitor, CS2 (500nM), for 7 days. *** $p=0.0009$ (**b**) and *** $p=0.0001$ (**c**), by paired two-tailed t test. **d**, Glutamate-induced excitotoxicity in control and *C9ORF72*-ALS/FTD iPSNs after DMSO or CS2 treatment. Different shapes represent different iPSN lines. **** $p<0.0001$ by paired two-tailed t test. **e**, A schematic model showing how global m⁶A hypomethylation in *C9ORF72*-ALS/FTD impairs neuronal function and results in neuronal death by stabilizing *C9ORF72* repeat RNA and dysregulating neuronal gene expression. Points represent individual patient iPSN lines. $n=6$ in each group. (**a-d**) Data are mean \pm s.e.m.